Coupled simulations of the mid-Holocene and Last Glacial Maximum: new results from PMIP2

P. Braconnot, B. Otto-Bliesner, S. Harrison, S. Joussaume, J.-Y. Peterchmitt, A. Abe-Ouchi, M. Crucifix, T. Fichefet, C. D. Hewitt, M. Kageyama, et al.

Clim. Past Discuss., 2, 1293–1346, 2006
www.clim-past-discuss.net/2/1293/2006/

Climate of the Past Discussions

Climate of the Past Discussions is the access reviewed discussion forum of *Climate of the Past*

Coupled simulations of the mid-Holocene and Last Glacial Maximum: new results from PMIP2

P. Braconnot[1], B. Otto-Bliesner[2], S. Harrison[3], S. Joussaume[1], J.-Y. Peterchmitt[1], A. Abe-Ouchi[4], M. Crucifix[5,6], T. Fichefet[6], C. D. Hewitt[5], M. Kageyama[1], A. Kitoh[7], M.-F. Loutre[6], O. Marti[1], U. Merkel[8], G. Ramstein[1], P. Valdes[3], L. Weber[9], Y. Yu[10], and Y. Zhao[3]

[1]Laboratoire des Sciences du Climat et de l'Environnement, Unité mixte CEA-CNRS-UVSQ, Orme des Merisiers, bât. 712, 91191 Gif-sur-Yvette Cedex, France
[2]National Center for Atmospheric Research, 1850 Table Mesa Drive, Boulder, Colorado, USA
[3]School of Geographical Sciences, University of Bristol, Bristol, BS8 1SS, UK
[4]Center for climate System Research, The Univ. of Tokyo, Japan 277-8568 and FRCGC/JAMSTEC, Yokohama, 236-0001 Japan
[5]Met Office Hadley Centre, Fitzroy Road, Exeter EX1 3PB, UK
[6]Université Catholique de Louvain, Institut d'Astronomie et de Géophysique Georges Lemaître, 1348 Louvain-la-Neuve, Belgium
[7]Meteorological Research Institute, Tsukuba, Ibaraki 305-0052, Japan
[8]Univ. Bremen, FB5 Geosciences, Geosystem modelling, P.O. Box 330 440, 28334 Bremen, Germany

[9]Royal Netherlands Meteorological Institute, PO Box 201, 3730 AE De Bilt, The Netherlands
[10]LASG, Institute of Atmospheric Physics, Chinese Academy of Sciences, P.O. Box 9804, Beijing 100029, P.R. China

Received: 6 November 2006 – Accepted: 1 December 2006 – Published: 13 December 2006

Correspondence to: P. Braconnot (pascale.braconnot@cea.fr)

Abstract

A set of coupled ocean-atmosphere simulations using state of the art climate models is now available for the Last Glacial Maximum and the mid-Holocene through the second phase of the Paleoclimate Modeling Intercomparison Project (PMIP2). This study presents the large scale features of the simulated climates and compares the new model results to those of the atmospheric models from the first phase of the PMIP, for which sea surface temperature was prescribed or computed using simple slab ocean formulations. We consider first the large scale features of the climate change, pointing out some of the major differences between the different sets of experiments. Then we quantify the latitudinal shift of the location of the ITCZ in the tropical regions during boreal summer. It is shown that this shift is limited for LGM, whereas a northward shift and an increase of precipitation are well depicted for mid-Holocene in continental regions affected by monsoon precipitation. In the last part we quantify for both periods the feedback from snow and sea-ice in mid and high latitudes. We show that it contributes for half of the cooling in the northern hemisphere for LGM, the second half being achieved by the reduced CO_2 and water vapour in the atmosphere. For mid-Holocene the snow and albedo feedbacks strengthen spring cooling and enhance boreal summer warming, whereas water vapour reinforces the late summer warming. These feedbacks are modest in the southern hemisphere. For LGM most of the surface cooling is due to CO_2 and water vapour.

1 Introduction

There is widespread concern about ongoing and future global environmental changes. Projections of possible future climate changes, under different assumptions, can only be made with numerical models of the earth system. The last IPCC report (IPCC, 2001) states that our confidence in the ability of models to project future climate has increased. Yet there are still significant discrepancies between different model results,

CPD

2, 1293–1346, 2006

both in terms of simulated climate changes and more fundamental aspects of the representation of internal processes and feedbacks. We therefore need to be able to evaluate whether the model results are reliable (or not), and also to attempt to estimate whether the models incorporate the required level of complexity to represent the range of possible responses of the coupled earth system.

The record of past climate conditions provides a unique opportunity to achieve these goals. Palaeodata present a many faceted challenge for our understanding of the natural variability of the climate system. The coupling of the different climate components through water, energy and biogeochemical cycles, and the link between trace gases, aerosols and climate all need to be considered to represent past changes and assess future climate change. Co-ordinated comparisons of data and model results of the Paleoclimate Modelling Intercomparison Project (PMIP) for key times in the past have provided grounds for confidence in some aspects of the models, while continuing to present important challenges (Joussaume and Taylor, 1995; PMIP, 2000). PMIP is a long-standing initiative endorsed by the World Climate Research Programme (WCRP; JSC/CLIVAR working group on Coupled Models) and the International Geosphere and Biosphere Programme (IGBP; PAGES). The major goals of PMIP are to determine the ability of models to reproduce climate states that are different from those of today and to increase our understanding of climate change (Joussaume and Taylor, 1995).

In its initial phase (PMIP1), PMIP was designed to test the atmospheric component of climate models (atmospheric general circulation models: AGCMs), under the last glacial maximum (LGM: ca 21 000 years before present, 21 ka) and the mid-Holocene (6000 years before present, 6 ka BP) conditions. The LGM simulation was conceived as an experiment to examine the climate response to the presence of large ice sheets, cold oceans and lowered greenhouse gas concentrations. The mid-Holocene simulation was designed as an experiment to examine the climate response to a change in the seasonal and latitudinal distribution of incoming solar radiation (insolation) caused by known changes in orbital forcing (Berger, 1978).

Many features of the PMIP1 experiments, including global cooling at the LGM and the

expansion of the northern hemisphere summer monsoons during the mid-Holocene, are robust in that they are both shown by all models and by palaeoenvironmental observations (PMIP, 2000). However, differences in the magnitude of the response between individual models are large. AGCMs forced by CLIMAP (1981) reconstruction of LGM sea surface temperature (SST), for example, fail to produce the magnitude of glacial cooling in the tropics shown by palaeoenvironmental observations (Farrera et al., 1999; Pinot et al., 1999b). However, although some of the atmosphere-mixed-layer ocean models produce tropical cooling of the right magnitude, others produce no greater cooling than the AGCM simulations (Harrison, 2000). Similarly, the simulated latitudinal expansion of the African monsoon at 6 ka BP is considerably smaller than shown by palaeoenvironmental observations: some models underestimate the precipitation required to sustain vegetation at 23° N in the Sahara by 50% while others fail to produce an increase in precipitation this far north (Joussaume et al., 1999). The PMIP1 results formed a crucial part of the evaluation of climate models in the Third Assessment Report of the Intergovernmental Panel on Climatic Change (MacAvaney et al., 2001).

The state-of-the-art models now include dynamical representations of the global atmosphere, ocean, sea-ice, and land surface, and the interactions among these components. Complementary experiments, examining the role of the ocean and of the land surface in past climate changes have also been carried out by several PMIP1 participating groups (see Cane et al., 2006). These experiments demonstrated that the ocean and vegetation feedbacks were both required to simulate the regional patterns and magnitude of past climate changes correctly. The focus on evaluation of coupled models against past conditions is timely because coupled ocean-atmosphere models (OAGCMs) have, in recent years, become the basic tool for projections of future climate change. Coupled ocean-atmosphere-dynamic vegetation models (OAVGCMs) have now been developed by several modeling groups and will be used for future climate projections. Coupled simulations also allow us to consider new questions such as the response of the thermohaline circulation (THC) and its impact on climate change,

or the changes in interannual to multidecadal variability and the role of ocean and vegetation feedbacks in modulating these changes.

The second phase of the project (PMIP2) was launched in 2002 (Harrison et al., 2002). The LGM and the mid-Holocene remain key benchmark periods for the project, for which respectively 6 and 9 modeling groups performed coupled ocean-atmosphere simulations following the same protocol. The objective of this overview paper is to highlight the large scale features of these simulations, and to compare the results with those of PMIP1 where possible. Several analyses have already considered the results of these new simulations, considering the polar amplification of temperature (Masson-Delmotte et al., 2006), model evaluation over the North Atlantic ocean and Eurasia at the LGM (Kageyama et al., 2006), climate sensitivity (Crucifix, 2006), the glacial THC in the Atlantic ocean (Weber et al., 2006), and tropical climate variability over west Africa (Zhao et al., 2006). Here we overview the results of the PMIP2 for LGM and mid-Holocene, highlighting change in global temperature, and in the hydrological cycle. We consider global indicators, as well as changes in the position of the ITCZ in the tropics and the role of the change in snow and sea-ice cover in mid and high latitudes.

Section 2 presents the PMIP2 protocol used to run the 21 ka and 6 ka coupled experiments, as well as the present state of the PMIP2 database. Section 3 compares the large scale features of PMIP2 simulations with those of PMIP1, and discusses the role of the vegetation feedback. Sections 4 and 5 respectively focus on the tropical and extra-tropical regions. Conclusions are provided in Sect. 6.

2 Simulations of the mid-Holocene and Last Glacial Maximum

2.1 Experimental protocol

As for PMIP1, a strict protocol is provided to run the PMIP2 21 ka and 6 ka experiments (see http://www-lsce.cea.fr/pmip2). It represents the best compromise between the

need to account for the different forcings and to have realistic boundary conditions that guarantee the relevant character of the model-data comparison, and pragmatic constraints imposed by the model structures and stability.

The reference (control) simulation (0 ka) is a pre-industrial (circa 1750 A.D.) type climate. The orbital parameters are prescribed to the references values of 1950 A.D. (as done in PMIP1), and trace gases correspond to 1750 A.D. In simulations with the OA version of the models, vegetation is prescribed for most models to the present day distribution of vegetation. This may potentially affect model-data comparisons, because the prescribed vegetation already accounts for land use. In OAV simulation, vegetation is interactively computed by the model and represents natural vegetation.

The major difference between 6 ka and 0 k arises from the orbital configuration (Table 1), which leads to an increase of the seasonal cycle of the incoming solar radiation at the top of the atmosphere (insolation) in the northern hemisphere of 23 W/m^2 and to a decrease in the southern hemisphere. The larger tilt also increases summer and annual mean insolation in the high latitudes of both hemispheres. Orbital parameters are derived from Berger (1978), and CH_4 concentration is prescribed as 650 ppbv. The concentrations of the other trace gases (CO_2 and N_2O) are kept as in the pre-industrial simulations. A first set of simulations is run with the OA version of the models. In these simulations vegetation is the same as in the control simulation, in order to determine the response of the ocean-atmosphere system to the changes in forcing. Simulations where the dynamical part of the vegetation model is activated (OAV simulations) are branched off the OA simulations. Thus, the role of vegetation and feedbacks due to vegetation can be analyzed.

Additional constraints are needed for the 21 ka simulations. The land-sea mask and topography are changed so as to correctly account for the ice sheets and the lowering of sea level. The ICE-5G global reconstruction of ice sheet topography (Peltier, 2004) was adopted (Table 2). Surface altitude in 21 ka experiments is calculated as 0 ka + (ICE-5G 21 ka – ICE-5G 0ka), where ICE-5G 21 ka and ICE-5G 0 ka are the reconstructions for 21 000 years ago and the present, respectively. The globally averaged

salinity of the LGM ocean is imposed to be the same as in the control simulation. Furthermore the experimental protocol recommends that net accumulation of snow over the northern ice sheets is compensated for by a freshwater input over the Arctic and north of 40° N in the Atlantic. This mimics iceberg melting and closes the freshwater balance. Moreover, changes in the river flow components should be accounted for, following as much as possible data based references. However, inter-model differences exist in the treatment of snow accumulation and river run-off (Weber et al., 2006).

The 21 ka simulation poses a major technical challenge because we need to bring the ocean circulation into a glacial state. To do this from the pre-industrial control simulation would require several thousand years of simulation. This is not feasible with complex models, and thus some form of acceleration technique or asynchronous-coupling of the fast atmosphere and slow ocean has to be employed to bring the model into a glacial state prior to running the LGM experiment. Several approaches have been suggested, but it is not clear which of these will produce the best results. Each of the modelling groups therefore uses its own "spin-up" technique to initialize and initiate the 21ka simulation.

For each time period and experiment, the models are run long enough for the trends over the final 100 years to be small. The last 100 or 200 years of experiments are considered for the analyses are uploaded in the common database. Mean seasonal cycle were computed for a 100 year averages.

2.2 Models and database

Results of the different simulations are stored in a common database hosted at LSCE on raid disks and the data is distributed through a Linux file server. Guidelines, file format convention, variable names and structures, and utilities are adopted in coordination with the Coupled Modelling Intercomparison Project (see http://www-lsce.cea.fr/pmip2).

For most of the modelling groups, the version of the GCMs used for PMIP2 is identical to the version used for future climate change predictions. All the atmospheric

components of the OA and OAV models participating in the project account for the effect of CO_2 and other trace gases in their radiative codes. They also all include a sea ice model in the oceanic component. Table 2 indicates the state of the simulations for the two time periods and provides references for the different models used. More simulations have been performed but are still subject of quality assessments before being uploaded into the database, and are therefore not considered here. In addition Earth system model of intermediate complexity have been included because they offer the opportunity to make lots of sensitivity experiments to test several aspects of the climate system in a more effecient way than GCMs.

For comparison, we also present model results from the PMIP1 database. The corresponding model references can be found in Joussaume et al. (1999) for mid-Holocene and Pinot et al. (1999a) for LGM. The PMIP1 simulations of mid-Holocene are atmosphere-only simulations (SSTf), for which sea surface temperatures are kept as they are in the modern climate and the only difference with 0k arises from the orbital parameters. For the LGM all simulations used the Peltier (1994) ICE-4G ice sheet, and imposed lower concentration of gases (200 ppm for CO_2). In a first set of simulations, the SSTs were prescribed to the CLIMAP (1981) reconstruction (SSTf), whereas in a second set SSTs were computed using a slab ocean model coupled to the atmospheric model (SSTc). Mean seasonal cycles were computed for a 10 year average.

3 Large scale features of the simulated climate

3.1 Last Glacial Maximum

As expected from the presence of the Fennoscandian and Laurentide ice sheets in the Northern Hemisphere and the lower CO_2 concentration in the atmosphere, the LGM climate is characterised by a large cooling (Fig. 1a) with maximum cooling (about –30°C) over the ice sheets in the Northern Hemisphere (NH). The ice sheet height and the large cooling alter the characteristics of the stationary waves, and contribute to

the large cooling (–5 to –10°C) downstream over the whole Eurasian continent. In the tropical regions the continental cooling is of smaller magnitude (–2 to –5°C). This moderate cooling is also found in most places over the ocean in mid-latitudes and in the tropical regions. The cooling does not exceed –2°C in several parts of the subtropical oceans in the Pacific and in the Southern Hemisphere (SH) in the Atlantic and Indian oceans.

Even though all OA simulations exhibit similar large scale features for the LGM cooling, significant differences are found in the magnitude of the response among the models. Figure 2 provides an indication of the model dispersion. The global mean range is –3.6 to –5.7°C amongst PMIP2 OA simulations. Interestingly, model dispersion is largest in the southern hemisphere where the cooling varies from –2 to –5.3°C depending on the model. This is due to large differences in the response of the circumpolar ocean and of the temperature over sea-ice. The latter varies from small cooling of –2°C up to –10°C when sea-ice cover increases all around the Antarctic continent. There is less dispersion in central Antarctica where Masson et al. (2006) report a –3.7 to –5.1°C range, consistent with ice core estimates. In NH the cooling is larger and model dispersion is smaller (2°C). The seasonal contrast is small, with only a 1°C difference in the magnitude of the NH cooling between DJF and JJAS (Fig. 2c).

Tropical oceans were warmer in PMIP1 simulations using CLIMAP (1981) SSTs (Fig. 1b), which explains why the global cooling was not as large in PMIP1 SSTf experiments (Fig. 2), ranging from –3.3 to –4.7°C. Also the 2°C spread in PMIP1 results is equivalent to the one found for the OA simulations in NH. This suggests that the mean difference between OA and SSTf experiments is due to the ocean cooling, whereas the model dispersion for a given set of simulations is mostly due to the continental cooling and the way feedbacks from snow, ice and clouds are treated in the different models. On the other hand, PMIP1 SSTf results in SH are more similar from one model to the other due to the stronger constraint of the prescribed SSTs in this hemisphere. The range of results is only slightly warmer than those of the OA simulations.

The geographical pattern of the annual mean cooling also exhibits systematic differ-

ences between PMIP1 SSTf and PMIP2 OA simulations in NH (Fig. 1). In particular, the maximum cooling in PMIP1 SSTf experiments is found over sea-ice in the North Atlantic and Nordic Seas and over the ice sheets, with a maximum over the Fennoscandian ice-sheet. In the PMIP2 OA simulations the sea-ice cover is not as large as in CLIMAP (1981). The maximum cooling is found on the Laurentide ice sheet (Fig. 1a), which could be due to the fact that this ice-5G ice sheet is higher than the ICE-4G reconstruction. The PMIP1 SSTc experiments produced global features more similar with the new OA experiments, except that they produce colder conditions over parts of the subtropical oceans, the North Atlantic and continental regions extending from North Africa to South-East Asia over the continent (Fig. 1c). This is mainly due to the responses of 3 of the models that produce a global cooling exceeding –6°C (Fig. 2).

The precipitation pattern (Fig. 1 right panel) is characterised by a large scale drying (up to –1 to –4 mm/d depending on the regions) resulting from the large scale cooling and reduced evaporation. PMIP2 OA simulations show that in both hemispheres at high latitudes the drying is largest over the ice sheets and sea ice (Fig. 1), while in the tropical regions it is affected by the seasonal variations of the Intertropical Convergence Zone (ITCZ). However, some regions in the mid-latitudes both in NH and SH experience larger annual mean precipitation (0.5 to 2 mm/d). This intensification of precipitation results from shifts in the major characteristics of the atmospheric dynamics, such as the southward shift of the storm tracks in NH mid-latitudes or changes in the southern hemisphere convergence zone.

A very different picture emerges from PMIP1 SSTf simulations where the drying extents over the continent and over the North Atlantic because of the large sea-ice extent. In addition regions of increased precipitation are found over the tropical ocean over the widely criticized warm pools of the CLIMAP reconstruction. The continental drying found from the PMIP1 SSTc simulations is similar to the PMIP2 OA results. Differences appear over the ocean at the eastern edge of the storm stracks in the Pacific and Atlantic oceans (Fig. 1). It was shown in PMIP1 that the storm tracks followed the southward shift of the sea-ice cover in the Northern Hemisphere (Kageyama et

al., 1999). Since the temperatures were very low in these simulations, the amount of water vapour was reduced in the atmosphere, and evaporation was very low at the surface. Therefore precipitation was strongly reduced in these simulations. In the case of PMIP2 OA simulations, the change in sea-ice cover is more limited, and the southward shift of the storm tracks follows the change in the meridional SST gradient. Since the cooling is not as large as in PMIP1 there is more water vapour in the atmosphere and evaporation still occurs along the path of the storm track, which explains the signature in precipitation.

3.2 Mid-Holocene

Changes are modest compared to those of the LGM, but reflect the sensitivity of the climate system to changes in the mean seasonal cycle of insolation. In particular, there is nearly no simulated change in annual mean temperature or precipitation for the mid-Holocene, consistent with no change in global annual mean insolation. The major changes for this period compared to present correspond to an enhanced (reduced) seasonal cycle of temperature in the NH (SH). The continental warming favours the deepening of the JJAS thermal low over land, which intensifies the low level winds and moisture transport from the tropical ocean to the continent, and thereby intensify monsoon system in the tropical regions (Joussaume et al., 1999; Kutzbach et al., 1993).

All models simulate an amplification of the mean seasonal cycle of NH surface temperature. In summer, this is characterised by increased surface air temperature over NH continents and in mid and high latitudes over the ocean and the Arctic (Fig. 3). The continental warming reaches a maximum of about 2°C in central Eurasia and over the Tibetan Plateau (Fig. 3a). Over the ocean the warming is in general less than 1°C, except in North Atlantic and in the Arctic where it is close to 1°C. The SH continents show warmer conditions (South America, South Africa and Australia), whereas the ocean is colder or similar to today. A slight warming is also depicted along the Antarctic continent, resulting from the reduction of the sea-ice cover. The region extending from West Africa to the north of India is colder than today. This is the signature of the enhanced

JJAS monsoon flow and increased precipitation (0.25 to 2 mm/day; Fig. 3 right panel). In these regions, the increased cloud cover and increased local recycling (evaporation) both contribute to cool down the surface (Fig. 3).

Even though all the models produce similar large scale patterns, differences in the magnitude of the warming are found from one OA simulation to the other. This is illustrated on Fig. 4 by the comparison of the NH JJAS warming produced by each of the OA PMIP2 simulations. Except for one cold simulation, model results range from 0.2 to 0.8°C (Fig. 4b). Interestingly, the model scatter is quite similar to the one found for PMIP1 SSTf simulations for which the modern SST induced a strong constraint on the response of the climate system over the ocean and in regions covered by sea-ice. This suggests that most of the differences between models are due to differences in the large scale warming over the Eurasian and American continents and northern Africa.

These differences between PMIP2 OA simulations and PMIP1 SSTf simulations over the ocean and in high latitudes are well depicted in Fig. 3. Both sets of simulations exhibit a similar continental warming. Over the high latitude oceans, warming doesn't exceed 0.5°C in PMIP1 SSTf simulations (Fig. 3c), reflecting the fact that sea-ice is prescribed to present day conditions in these simulations. In the coupled simulations the reduced sea-ice cover induces the well known albedo feedback. The reduced sea ice cover in the coupled simulation reduces the surface albedo thus allowing solar radiation to warm the surface ocean and thereby to melt sea-ice from below. This feedback is further enhanced when the dynamic of vegetation is accounted for in the simulations, because snow albedo is reduced with higher vegetation (not shown). The feedback from vegetation and ocean thus translate the seasonal insolation forcing into an annual mean warming north of 40° N (Ganopolski et al., 1998; Wohlfahrt et al., 2004).

In winter (DJF) the major changes correspond to a large continental cooling with maximum values within the subtropical regions where the change in insolation is the largest (not shown). This contributes to strengthen the DJF winter monsoon, so that the NH continents experience drier conditions, whereas precipitation is reinforced over the

ocean (Braconnot, 2004; Cane et al., 2006). Figure 4 shows that the differences in the simulated NH DJF cooling between different models are larger for PMIP2 OA than for PMIP1 SSTf simulations. For the latter, the prescribed SST and sea-ice cover exert a strong constraint on the change in tropical ocean temperature and on the temperature over sea-ice. In most of the PMIP2 OA simulations a reduction of sea ice favours warmer conditions over the Arctic. In particular two of the models show a slight NH warming (Fig. 4).

4 Tropical regions and location of the ITCZ

Both paleo climates considered in PMIP2 are characterised by large changes in the hydrological cycle in the tropical regions (Figs. 1 and 3). In the following, we consider successively the change in the mean position of the ITCZ, the intensity of the African and Indian monsoons and discuss key feedbacks for the African monsoon during mid-Holocene.

4.1 Location of the ITCZ

Changes in precipitation inferred from proxy indicators tend to be often attributed to shifts in the mean position of the ITCZ. Analyses of LGM changes in precipitation from PMIP1 simulation over Africa suggested depleted rainfall in the ITCZ, with nearly no shift in ITCZ location (Braconnotet al., 2000a). On the other hand, results for 6 ka suggested that the northern limit of precipitation shifted indeed to the north over the Sahel region, but that for most models the core of the ITCZ remained in a position similar to today (Braconnot et al., 2000a; Joussaume et al., 1999). Mid-Holocene changes in precipitation result either from a change in the intensity of the convection or from a slight enhancement of the precipitation on the northern flank of the ITCZ (Joussaume et al., 1999). We thus use the set of PMIP1 and PMIP2 simulations to investigate how the location of the ITCZ changes for LGM and mid-Holocene and to

analyse if the ocean feedback has an impact on this diagnostics. We illustrate this point using summer conditions.

There is no robust criterion to define the northern limit of the ITCZ from precipitation. The reason is that the background level of precipitation varies a lot from model to model, and that some models produce spurious precipitation in arid regions (Braconnotet al., 2000a). Therefore we consider the core of the ITCZ in its northern part rather than the northern limit of the ITCZ. For each longitude we computed the latitudinal location of the centre of gravity of precipitation for precipitation located to the north of the maximum precipitation (peak of the ITCZ). The mean location is therefore provided by:

$$\text{loc\_ITCZ(lon)} = \frac{\sum_{y=\text{lat(pr max)}}^{30^\circ\text{N}} \text{pr(y)lat(y)}}{\sum_{y=\text{lat(pr max)}}^{30^\circ\text{N}} \text{pr(y)}},$$

where lon stands for longitude, lat, for latitude, pr for precipitation and prmax for the maximum precipitation. We computed the location of the ITCZ for each model on its own model grid. Figure 5 reports for each model the northern most position (loc_ITCZ(lon)) reached during JJAS for each longitude. Because of the different model resolution in longitude, some models contribute for more points in this figure. In order to evaluate if the location of the ITCZ is properly represented by the models, we apply the same procedure to the CMAP climatology (Xie and Arkin, 1996) and include it (red line) on each of the graphs of Fig. 5.

The comparison of PMIP2 OA results for 0k with climatology shows that most OA models capture the location of the ITCZ quite well (Fig. 5a). The major deficiencies occur over Africa where the ITCZ is located too far south in two simulations and over the Indian ocean. In this region, one of the model favours convection over the ocean at the expense of the continent. Interestingly results of this subset of coupled models are in better agreement with the climatology than PMIP1 SSTf or SSTc simulations performed several years ago (Figs. 5b and c). In these earlier simulations the location

of the ITCZ is not well reproduced over the ocean and model to model differences can reach up to 20° in latitude. The scatter is even larger over the ocean for slab ocean models. This is particularly true over the West Pacific. Several models locate the ITCZ too far north over West Africa, mainly in the PMIP1 SSTf experiments (Joussaume et al., 1999).

At first look it is difficult to distinguish notable changes in the location of the ITCZ from PMIP2 OA LGM simulations (Fig. 5, right pannel). The reason is that the scatter between model results for preindustrial (0 ka) is larger than the ITCZ change simulated for LGM. Therefore, for each of the models, we plotted the magnitude of the LGM shift in latitude of the ITCZ as a function of longitude on Fig. 6. This shift is simply defined as:

$$\Delta\text{lat} = (\text{loc\_ITCZ(lon)})_{\text{LGM}} - (\text{loc\_ITCZ (lon)})_{\text{CTRL}}$$

Figure 6 also includes for each model as a function of longitude the change in precipitation averaged over the northern edge of the ITCZ, defined as:

$$\Delta\text{pr(lon)} = \left(\frac{\sum_{y=\text{lat(pr max)}}^{30^\circ\text{N}} \text{pr}(y)dy}{\sum_{y=\text{lat(pr max)}}^{30^\circ\text{N}} dy} \right)_{\text{LGM}} - \left(\frac{\sum_{y=\text{lat(pr max)}}^{30^\circ\text{N}} \text{pr}(y)dy}{\sum_{y=\text{lat(pr max)}}^{30^\circ\text{N}} dy} \right)_{\text{CTRL}},$$

where *dy* represents the length in latitude of each model grid box. These diagnostics show that some of the models simulate a slight southward shift of the ITCZ over the continents and the Indian Ocean. Note that one of the models (crosses in Fig. 6) is more sensitive than the others over Africa with about 5 to 8 degrees latitude difference compared to 0 ka. Other models show a northward shift over West Africa. The southward shift is more consistent between models over South America and near 130° E. However for the latter region some models exhibit a northward shift up to the foothills of Himalaya. Note that across the Pacific ocean the tendency is for a slight southward

shift in the eastern part and northward shift in the western part. Interestingly, event though the LGM climate is characterised by a drying in regions under the influence of the ITCZ, the mean amount of precipitation simulated on the northern edge of the ITCZ is only slightly reduced. The larger reduction occurs over Africa (20° W–40° E), the Indian and Asian monsoons (70° E–110° E) and South America 60° W–80° W). Note a tendency for increased precipitation over Southeast Asia and the West Pacific.

In contrast, PMIP1 SSTf and SSTc LGM simulations produce a larger northward migration of the ITCZ in the Pacific ocean (Fig. 5). For PMIP1 SSTf simulations this coincides with the warm pool of the CLIMAP SST over which evaporation is still active and precipitation is enhanced (Fig. 1). Results of SSTc experiments lie in between PMIP2 OA and PMIP1 SSTf results. Systematic differences compared to PMIP2 OA simulations remain, such as the northward shift across the Pacific. The comparisons of these different set of simulations suggest that the change in the ocean circulation has a large impact on the hydrological cycle in the tropical regions and strongly influence the mean position of the ITCZ, by reducing its latitudinal shift over the ocean.

Figures 6 and 7 show the same diagnostics computed for the mid-Holocene. Control simulations are also reported in Fig. 7, because they correspond to a different subset of models than the one considered for LGM, and also include models of lower resolution and of intermediate complexity. In particular, some of the additional simulations included in this set have a tendency to locate the modern ITCZ too far north over West Africa and the Panama isthmus. One of the models is clearly outside the range of the others and of data, suggesting that the ITCZ is located in the middle of the Sahara. Figure 6 shows that for mid-Holocene a northward shift of the ITCZ is simulated by almost all models over Africa, and in the Indian sector up to 130° E. It reaches 3 to 10 degrees latitude depending on the region. It is associated to an increase of the mean precipitation simulated over the northern edge of the ITCZ. On average this increase is 2 to 4 mm/d over Africa and three of the models simulate an increase larger than 6 mm/d over the Indian monsoon region. A southward shift of the ITCZ is also simulated over South America where precipitation decreases by 2 to 4 mm/d, following

results reported by Dias et al. (2006)[1]. The Indian sector is the region where the larger scatter is found between models. In this sector, the modern ITCZ oscillates during boreal summer between an oceanic and continental position (Gadgil and Sajani, 1998). Some of the models favour the ocean location at 6 ka. Note that there is no relationship between the change in the location of the ITCZ and the change in the amount of precipitation. This is seen by the fact that the sign on the Δlat and Δpr plotted on Fig. 6 are different for a southward shift and a decrease precipitation, which means that different models are concerned by these two aspects.

Comparison with PMIP1 simulations indicates that these broad features were already present in PMIP1 SSTf simulations, but that the northward shift was of smaller magnitude, at least over West Africa (Fig. 7). This is consistent with previous comparisons of coupled OA simulations of the mid-Holocene (Braconnot et al., 2004). As for LGM, large differences are found over the West Pacific, but they result mainly from differences in the control simulations. This stresses once more that biases in the control simulations may strongly impact the model response to a given forcing and that they should be considered when discussing mechanisms of climate change.

4.2 The African monsoon and Asian monsoon

The analysis of the maximum latitude reached by the core of the ITCZ during JJAS shows that this location is affected by the climate change only in some regions, such as Africa and the West Pacific. However the intensity of precipitation is quite different depending on the period analysed, with large change occurring over continual regions affected by monsoon precipitation. These regions have already been the focus of several studies within the PMIP project (Braconnot et al., 2002b; Joussaume et al., 1999; Liu et al., 2004; Zhao et al., 2005), which is why we compare the JJAS changes in pre-

[1]Dias, P. L., Dias, M. A. F., Braconnot, P., Turcq, B., and Jorgetti, T.: Evaluation of Model Simulation of 6 ka BP and Present Climate in Tropical South America, Clim. Dyn., submitted, 2006.

cipitation over West Africa (20° W–30° E, 10° N–25° N) and North India (70° E–100° E, 20° N–40° N) for the two periods and all sets of experiments (Fig. 8). These regions are defined as in Zhao et al. (2005).

The change in JJAS precipitation over West Africa ranges from 0.2 mm/d to 1.6 mm/d for mid-Holocene OA simulations (not shown). It represents an increase of about 5 to 140% compared to present day rainfall in this region (Fig. 8). Both OA and OAV simulations tend to produce larger precipitation change in this region than PMIP1 SSTf experiments. This increase in precipitation is due to the response of the ocean and the building up of warmer conditions in the subtropics and mid latitudes in the Atlantic north of the equator and colder conditions in the southern hemisphere (Fig. 3). This strengthens the cross equatorial flow and favours the maintenance of the ITCZ to the north of its present day position in West Africa and the nearby ocean (Braconnot et al., 2000b; Kutzbach and Liu, 1997; Zhao et al., 2005). In comparison OA simulations produce a modest increase of monsoon rain (0.2 to 0.8 mm/d) to the North of India corresponding to a 5 to 33% increase of precipitation in this region (Fig. 8b). The relative changes in monsoon are thus less important in India than in Africa. Comparison with PMIP1 simulations shows that contrary to what happens for Africa, the ocean feedback contributes to reduce the mid-Holocene monsoon amplification. Liu et al. (2004) and Ohgaito and Abe-Ouchi (2006)[2] proposed that surface wind convergence over the warmer western tropical North Pacific competes with the insolation-induced increase in convergence and moisture transport into India and therefore substantially reduces Indian monsoon rainfall. Zhao et al. (2006) further suggest that the colder than present day SST anomaly in spring in Arabia Sea leads to less moisture supply and thereby to a decreased in Indian monsoon precipitation.

During the LGM both regions experienced drier conditions (Fig. 8b). Results from the OA simulations suggest a reduction of about 20 to 42 % over Africa, except for one model that produces a slight enhancement of precipitation (+16%). A group of PMIP1

[2]Ohgaito, R. and Abe-Ouchi, A.: The role of ocean thermodynamics and dynamics in Asia summer monsoon changes during the mid-Holocene, Clim. Dyn., submitted, 2006.

SSTf simulations produce larger reduction in precipitation, up to a 62%. Interestingly the spread of PMIP1 SSTc results is even larger with two extreme models reaching a reduction of 80%, and three models for which the reduction in precipitation does not exceed 10%. Over North India, similar conclusions can be drawn (Fig. 8c). The change in rainfall is however slightly less than over Africa. The comparison of the results of the different sets of simulations suggests that the ocean feedback do not play a local role in the reduction of continental precipitation. The change in precipitation is therefore mostly due to the change in the mean water vapour across the tropical regions, resulting from changes in atmospheric water vapour, residence time of water in the atmosphere and changes in water vapour advection.

Several studies have attempted to relate the change in precipitation simulated for past conditions to model characteristics for present day. For example Joussaume et al. (1999) show that models that produce the change in precipitation the furthest north over Africa are also those that simulate the present day ITCZ the furthest north. However, it was not possible to establish a clear relationship between the amount of precipitation simulated for the control simulation and the amount of precipitation change for mid-Holocene (Braconnot et al., 2000). This is summarized here by plotting the ratio of precipitation change as a function of the precipitation of the control experiments for the African and Indian boxes (Fig. 9). Interestingly, such a relationship is found for PMIP2 OA simulations over these two regions. The relationship is even counter intuitive. Models that produce the largest precipitation for present day tend to produce less change for mid-Holocene. This suggests that the monsoon system is already saturated in the control simulations and that it is not possible to enhance much further. More investigation is needed to fully explain it.

For LGM such relationships (no show) are not valid. Model results are more different, may be due to the larger dependence of the results on changes in water vapour and radiative effects in the tropics. Models span a wide range of responses, as they do for future climate (Douville, 2006).

4.3 Discussion of some identified feedbacks for the mid-Holocene

Monsoon changes over Africa have been widely studied during PMIP1 and with previous versions of OA and OAV models by individual groups. These studies lead to the conclusion that both ocean and vegetation feedbacks were needed to represent the moist conditions reported from data in the Sahel region (Braconnot et al., 1999; Braconnot et al., 2004). Here, the new PMIP2 simulations with interactive vegetation only slightly increase rainfall compared to OA simulations (Fig. 8). Vegetation feedback seems thus less important than it was stated from previous AOV experiments (Braconnot et al., 1999) or from coupled atmosphere-vegetation experiments (e.g. Claussen and Gayler, 1997; Texier et al., 1997). Part of it is due to the differences between the OA and OAV control experiments for the same model. Indeed, in order to quantify the vegetation feedback without ambiguity, one should compare the OAV 6 ka experiment with an OA 6 k experiment for which the vegetation is prescribed the vegetation simulated in the OAV 0k experiment, as suggested by the PMIP 2 protocol. These simulations are not available yet in the PMIP2 database. Here for a given model, the OA and OAV experiment for 6 ka do not share the same control experiment. The three models simulate respectively 4%, 13% and 19% less precipitation in the monsoon region in the OAV 0 ka simulations compared to the corresponding OA 0 ka simulation (not shown). For two models this difference is as large as the difference between mid-Holocene and present. The interactive vegetation in the control climate induces land surface conditions in favour of a drier climate. The same processes may operate in the mid-Holocene simulation, explaining why the impact of vegetation is small. For example part of the differences could result from soil moisture and/or from interactions between vegetation and soil, which was shown by Levis et al. (2004) to limit the role of interactive vegetation. Additional analyses are needed to fully understand this result.

On the other hand, comparison of PMIP1 and PMIP2 simulations confirms that the ocean feedback strengthens the African monsoon. We further confirm here that the more models enhance the meridional SST gradient in the tropical Atlantic the more

they simulate an increase in precipitation over West Africa (Fig. 10). To analyse this we computed the canonical correlation between tropical Atlantic SST and Sahel precipitation for the mean seasonal cycle of the difference between 6 ka and 0k following the method developed by Zhao et al. (2006) in their analysis of interannual variability. We consider each model result as an independent realisation of the seasonal cycle. The second vector (Fig. 10) is representative of summer conditions with warmer SST to the north of 5° N and colder SST to the south of 5° N. The corresponding pattern of precipitation over land highlights the increased mid-Holocene precipitation to the north of 10° N. For each the model we extracted the value of the corresponding time series for JJAS for the ocean and the precipitation pattern respectively. The relationship between the JJAS value of the corresponding time series for SST and precipitation for each model clearly show a linear trend across the models, with higher values for models with larger increase in SST gradient and larger change in precipitation over land. This result confirms the role of the ocean in triggering the monsoon trough and the advection of moist air from the ocean into the continent (Zhao et al., 2005). This mechanism is only active in the Atlantic Ocean.

5 Mid and high latitudes snow and sea-ice feedback

Changes in the snow cover and sea-ice cover have direct effects on surface albedo and thereby on the radiative heat budget and temperature. For example, the large ice sheets present in the northern hemisphere during LGM contribute about –3.3 to –2.0 W/m^2 of the radiative cooling at this period (Taylor et al., 2000, 2006). The resulting cooling, in turn, increases the snow and ice cover which further contributes to cool down the system. These effects are large in mid and high latitudes. Feedbacks from snow and sea-ice are also expected for mid-Holocene at the seasonal time scale. In this section, we investigate from PMIP2 and PMIP1 how changes in snow and sea-ice cover influence climate between 30° and 90° latitude in both hemispheres. The analyses first consider the changes in snow and ice for both time periods and then

evaluate the impact of these changes on the top of the atmosphere heat budget.

5.1 Changes in snow and sea-ice cover

In addition to the increased continental ice sheets at LGM, which account for about 12% of the NH ice cover north of 30° N, the LGM simulations show increased snow cover ranging from 10 to 30%. Two PMIP2 OA LGM simulations show a larger increase during summer time (not shown). In PMIP1, on the contrary, the changes in snow cover are about 10% smaller than in the OA models and exhibit no seasonal variation (not shown). The sea ice cover in the NH is also increased in the PMIP2 OA LGM simulations, by about 5% in 3 models (Fig. 11). One simulation exhibits a larger change (up to 10%) from January to October. In the SH, all OA models, except one, suggest a change in the sea-ice seasonal cycle with large increases in October-November. One model produces a uniform 20% increase with no seasonal cycle. The major difference with PMIP1 experiments is the seasonality of the change. In PMIP1, even though the same boundary conditions were imposed in all the models, the interpolation on the model grid and in time between the minimum and maximum values provided by CLIMAP lead to slightly different sea-ice cover from one model to the other, reaching as much as 10% difference (Fig. 11 bottom, blue curves). Interestingly in the southern hemisphere sea-ice was larger during summer and smaller during winter in the PMIP1 simulations. On the other hand, SSTc simulations produced very different sea-ice cover with some of the models suggesting up to 25% more sea-ice in NH (red curves). Note also that in both hemispheres, the PMIP2 simulation with interactive vegetation (red) produces enhanced sea ice (by a few %) compared to the corresponding OA simulation.

During the mid-Holocene, changes in snow and sea-ice cover are more contrasted from one season to the other. The general feature simulated by both PMIP2 OA and PMIP1 SSTf is larger snow cover in March and May in the NH (Fig. 12), due to the smaller insolation. In boreal summer the melting is larger than today. The change in the building up of the snow cover from October to May occurs in two phases, one in

October–November and the other one from February to May. PMIP2 OA simulations produce a larger enhancement of the snow cover in spring than PMIP1 SSTf (Fig. 12). This can be attributed to the colder conditions induced by the ocean response to the insolation forcing. However, the retreat of the snow pack occurs earlier and conditions with less snow than today last until October. This latter point is consistent with the late warming of the ocean in autumn, which favours warmer conditions in the northern hemisphere. Simulations with interactive vegetation enhance this feature, certainly due to the warmer condition in mid and high latitudes favoured by the northward migration of forest. Changes in sea ice cover for the mid-Holocene OA simulations are shown in Fig. 13. The sea-ice cover is slightly reduced year round in the NH in all PMIP2 OA simulations except one (Fig. 13), with a pronounced decrease (2 to 25%) during summer and early autumn (JASO). In the SH, sea ice cover is much less affected by insolation changes, except for one simulation where it is reduced by about 10%. However the slight decrease of sea-ice during DJF is consistent with increased insolation in high latitude resulting from the larger obliquity. Indeed, even though precession contributes to damp the seasonal cycle in the southern hemisphere, obliquity increases it annually and seasonally.

These analyses suggest that for the NH, snow cover changes during the mid-Holocene should have a major impact in spring, whereas sea-ice changes should have a larger impact during summer. Changes in snow and sea-ice should not affect the radiative budget of mid and high latitude in the southern hemisphere.

5.2 Radiative impact of snow and sea-ice cover

In order to check if we can detect the impact of the changes in snow and sea-ice cover on the radiative budget of mid-and high latitudes, we compute the change in radiative heat budget at the top of the atmosphere (TOA) averaged from 30° N to 90° N and 30° S to 90° S respectively:

$$\Delta\mathrm{TOA} = (\mathrm{SWn}_{\mathrm{pal}} - SWn_{0\,\mathrm{k}}) - (\mathrm{LWn}_{\mathrm{pal}} - \mathrm{LWn}_{0\,\mathrm{k}})$$

where ΔTOA represents the change in net radiative heat flux at the top of the atmosphere, SWn represents the net shortwave radiation at the top of the atmosphere (positive downward) and LWn the net longwave radiation (positive upward). The indices pal refers to the past period considered (21 ka or 6 ka). In this analysis we consider only 3 models for which radiative fluxes for all sky and clear sky (*cs*) are available in the database for the two time periods. We also make simple approximations to obtain the first order of magnitude of the change in net heat flux at the top of the atmosphere (TOA) considering the change in short (SWn) and long wave fluxes (LWn). We quantify the role of clouds using the cloud radiative forcing (crf):

$$\mathrm{cfr} = \mathrm{TOA} - \mathrm{TOAcs}, \quad \mathrm{crfsw} = \mathrm{SWn} - \mathrm{SWncs}, \quad \text{and} \quad \mathrm{crflw} = \mathrm{LWn} - \mathrm{LWncs}$$

A more complete heat budget should also consider the heat transport at the equatorward boundary of each region, but we do not consider this aspect here. As a first approximation we assume that the paleo change in shortwave for clear sky is primary due to surface albedo. However, even though the same change in insolation (ΔSWi) is provided to all models at the top of the atmosphere, the forcing is different among the models because they use different planetary albedo for the preindustrial control simulation ($\alpha_{0\,\mathrm{k}}$). The shortwave forcing (SWf) is estimated following Hewitt and Mitchell (1996) :

$$\mathrm{SWf} = (1 - \alpha_{0\,\mathrm{k}})\,\Delta\mathrm{SWi}$$

This effect has to be accounted to estimate the change in SWncs induced by changes in snow and sea-ice cover. The latter is thus provided by:

$$\left(\mathrm{SWn}cs_{\mathrm{pal}} - \mathrm{SWn}cs_{0\,\mathrm{k}}\right) - \mathrm{SWf},$$

In addition, it is difficult with standard model output to make a clear estimate of the role of water vapour and of temperature on the longwave flux. We make the assumption that the difference between the emission from the surface and the top of the atmosphere represents the greenhouse effect of the atmosphere (g). The greenhouse effect is

mostly affected by greenhouse gases and water vapour. The effect of the change in surface temperature (T) and of the atmospheric greenhouse effect on LWn are then simply estimated by (Meehl et al., 2004):

$$\Delta\text{emisT} = 4\sigma T_{0\,\text{k}}^3 \left(T_{s\text{pal}} - T_{s0\,\text{k}}\right) \quad \text{and} \quad \Delta g = \left(\sigma T_s^4 - \text{LWncs}\right)_{\text{pal}} - \left(\sigma T_s^4 - \text{LWncs}\right)_{0\,\text{k}}$$

These estimates are plotted for LGM and mid-Holocene on Figs. 14 and 15 for NH and SH respectively. Several features emerge from these figures. First at LGM the net clear sky heat flux at TOA is negative in annual mean for the region north of 30° N, but this masks a slight increase in the TOAn compared to present day from October to March (Fig. 14a). The reason of this positive change in net heat flux is that the albedo of the ice-sheet has only little impact during this season, since solar radiation is very small (Fig. 14). Therefore the signal is dominated by the reduction of long wave emission. The latter is nearly constant over the year (–10 to –15 W/m^2). During March to September the change in shortwave radiation is dominant and the increased albedo contributes to the net cooling of the system (about –40 W/m^2 in June–July, Fig. 14c). If we consider to first approximation that ice-sheets, sea-ice and snow have similar albedoes, then $^1/_4$ of this change is due to the ice-sheet forcing and $^3/_3$ to the feedback from snow and sea-ice. The ice sheet forcing corresponds to about 10% of the change in SWncs (Fig. 14c). Estimations of this term using the approximate partial radiative perturbation method developed by Taylor et al. (2006) vary from –7 to –14 W/m^2 in annual mean depending on the model. Therefore we estimate from Fig. 14c that the feedback from snow and sea-ice varies from about 3 W/m^2 during boreal summer to about 30 W/m^2 during boreal winter. This effect is thus larger than the effect of the changes in cloud estimated by the cloud radiative forcing (Fig. 14b). Note however that estimations of cloud radiative forcing is ambiguous over highly reflecting surfaces (Bony et al., 2006). Cloud radiative forcing suggests a small impact of the change in clouds on the heat budget, with a tendency to counteract the radiative cooling (Fig. 14b). Our rough estimates of the origin of the change in the longwave heat flux at TOA also suggest that the dominant term is due to the surface cooling (–30 W/m2). The

reduction of the atmospheric heat gain, resulting from reduced CO_2 concentration and water vapour represents half this value. Therefore it suggests that ice sheet albedo, and CO_2 and water vapour each contribute equal parts of the cooling of the NH.

Conditions are different over the southern hemisphere (south of 30° S) where changes in the LGM net heat budget are much smaller (Fig. 15). The reason is that changes in ice-sheets and sea ice cover are less effective (Fig. 11). For these latitudes, the surface albedo has only small impact (Fig. 16c), except for the model (Fig. 13) that has the largest change in sea-ice cover. It is interesting to note that the reduction of the atmospheric heat gain is as large as the surface cooling, which shows that CO_2 and water vapour contribute most to the cooling at mid and high latitudes of the SH. This is consistent with several studies which suggested that the polar amplification over Antarctica provides a good constraint on climate sensitivity (Manabe and Broccoli, 1985; Masson-Delmotte et al., 2006), even though the relationship is complex (Crucifix, 2006).

For the mid-Holocene, changes in SWn also provide the dominant contribution to the seasonal heat budget of the mid and high latitudes (Figs. 14 and 15), primarily from changes in solar forcing. The net heat flux is thus reduced during winter north of 30° N and enhanced during summer. Figure 14f shows that the feedback from snow and sea-ice lead to about 2 to 5 W/m^2 additional reduction in SWncs in March (when snow cover is enhanced compared to present day) and an additional increase of about 5 W/m^2 during boreal summer when sea ice cover is reduced (Fig. 13). For both seasons, the changes in cloud forcing tend to counteract the solar forcing and surface albedo feedback (Fig. 14e). The role of decreased sea-ice cover and of surface warming during boreal summer has an impact on the atmospheric heat gain. The change in long wave radiation due to the change in temperature lag by about one month the insolation forcing and ice and snow SW feedbacks (Fig. 14f). Changes in the atmospheric heat gain show a slight reduction in May and increase during boreal summer when temperature is maximum. This results in increased temperature and increased water vapour in these regions, consistent with the response of the sea-ice, water vapour and

temperature to increased insolation forcing occurring after the summer solstice (Khodri et al., 2005). This effect is important compared to the magnitude of the other fluxes, and shows that water vapour feedback at high latitudes in the NH in strengths the warming. Similar lags between solar radiation, the role of surface albedo, temperature and water vapour are seen in the SH although of smaller magnitude (Fig. 15).

6 Conclusions

This comparison confirms previous conclusions found during the first phase of PMIP (PMIP, 2000), but also shows that for both the LGM and mid-Holocene the new generation of coupled models indicate systematic differences with PMIP1 SSTf or SSTc simulations.

PMIP2 OA simulations for LGM are colder than PMIP1 SSTf simulations, mainly because the simulations are colder in the tropical regions. Work in progress (Otto-Bliesner et al., personal communication, 2006) suggests that these new simulations are in general agreement with new tropical SSTs reconstructions from the MARGO project (Kucera et al., 2005). Systematic differences with earlier simulations are also found in the locations of the maximum cooling in the northern hemisphere over the ice-sheet, which also translate to differences in the change in precipitation along the NH storm tracks. The change in SST gradient in the North Atlantic and the cooling over Eurasia is consistent with data (Kageyama et al., 2006). The LGM climate is characterised by a large scale drying. In the tropical region, the African and Indian monsoons regions receive less precipitation than at present. These changes are very similar to the results found from PMIP1 SSTf and SSTc experiments, which suggests that the dominant factors contributing to the drying are the reduction of evaporation over the tropical ocean, and the reduction of the inland moisture transport. The position of the ITCZ varies only by a few degrees at LGM compared to its modern position, and the sign of this variation is model dependent over the continents. Over the oceans, the simulated changes in LGM SST are quite uniform so that PMIP2 OA simulations

exhibit similar northward extent of the ITCZ over the West Pacific as found in PMIP1 LGM experiments. The atmospheric water vapour is also reduced in mid and high latitudes. This reduction together with the reduction of the atmospheric concentration in CO_2 contributes the cold LGM climate. In the NH the large ice sheet albedo is the dominant forcing term. We estimate that for latitudes north of 30° N the feedback from snow and sea-ice represent about twice the ice sheet forcing. Albedo has thus a dominant role in the NH cooling and the reduction of the atmospheric greenhouse effect contributes only 50% of the albedo effect. In the southern hemisphere, on the other hand, albedo changes are small and the cooling is mainly driven by reduced CO_2 and water vapour.

For the mid-Holocene, the new results confirm that the response of the ocean and sea-ice shape the changes in the seasonal cycle of the surface air temperature and precipitation. The sea-ice has a large effect in high latitude, and in particular in the NH where its reduction during boreal summer strengthens the warming. In the tropical regions, the monsoons are enhanced both over West Africa and over the north of India. In these regions our analysis of the location of the ITCZ shows that the ITCZ shifts by several degrees northward and that precipitation is enhanced in the northern part of the ITCZ. The ocean feedback strengthens the response of the African monsoon and damps the response of the Indian monsoon. This results from different responses of the circulation in the Atlantic and Indian-Pacific sectors. In both regions, the cold ocean in spring strengthens the land-ocean contrast, and thus the moisture flux from the ocean to the continent. In the Atlantic this contrast is further enhanced by warmer than present SST north of 5° N and colder conditions south of 5° N, which favours a northward shift of the ITCZ over the Atlantic ocean and over the continent. We clearly establish that there is a positive relationship between this ocean response and the change in precipitation over West Africa. In the Indian sector, low level winds tend to converge over the warmer western tropical North Pacific, so that less moisture is transported to India, Therefore, the PMIP2 OA simulations produce less increase in Indian monsoon rain than the PMIP1 simulations with SST prescribed to the modern values.

Feedbacks from snow and sea-ice add to the NH mid-Holocene cooling induced by isolation changes in spring. Snow feedback is larger in the PMIP2 OA simulations than in the PMIP1 simulations. Also the melting of sea-ice in NH during mid-Holocene boreal summer impacts both surface albedo and the water vapour in the atmosphere. These two effects strengthen the late summer warming induced by the late response of the ocean to the increased insolation.

Our analyses also suggest that some of differences between PMIP1 and PMIP2 experiments could be attributed to the pre-industrial simulations. For pre-industrial conditions, the PMIP2 OA simulations better reproduce the location of the ITCZ than the previous generation of atmospheric models used in PMIP1. Note however that in DJF most of the coupled simulations produced a well marked doubled ITCZ structure in the east Pacific, and because of this are less satisfactory than the atmosphere alone simulation in this ocean basin for this season. In the PMIP2 OA simulations, a relationship is found for mid-Holocene between the ratio of the precipitation change and modern precipitation over West Africa and North India. Such relationship is not found for PMIP1 simulations, nor for the LGM climate. This needs to be investigated further and stresses that the large scale dynamics play an important role in redistributing precipitation during the mid-Holocene. In JJAS, precipitation is depleted over the ocean at the expense of the continent (Braconnot, 2004; Cane et al., 2006). During LGM, thermodynamics and reduced water vapour in the tropical regions seems to be the leading term to explain changes in monsoon rain. It is also not possible to establish a clear conclusion on the role of the vegetation feedback from the OAV simulations. The new PMIP2 OA simulations for the mid-Holocene confirm that vegetation feedback strengthens the African monsoon and the high latitude warming. However the magnitude of the feedback is smaller than previously discussed. Part of it comes from differences between OA and OAV pre-industrial simulations, such that further work is needed to provide robust conclusions.

The analyses of these simulations are just started, and new analyses are expected in the coming months. In particular, the role of the ocean and of its variability will

be further investigated looking at the changes in the thermohaline circulation and in the interannual variability. These new studies also require development of specific methodology to be able to compare model results with ocean data, or to infer the signature of interannual variability from the terrestrial proxy records. New periods of interest are also emerging. Some of the PMIP participants are interested in the Early Holocene, when the insolation forcing was even larger than during the mid-Holocene, and in glacial inception to better constrain the major feedbacks that are needed to amplify the insolation forcing and bring the system from a warm interglacial state to a cold glacial state. The comparison of the model results and model and data comparisons should help to better quantify the feedbacks from ocean, vegetation, snow and sea-ice and to test if the models have the right climate sensitivity, analysing not only mean climates, but also climate short term variability (interannual to multidecadal).

Acknowledgements. We acknowledge the international modeling groups for providing their data for analysis, the Laboratoire des Sciences du Climat et de l'Environnement (LSCE) for collecting and archiving the model data. The PMIP2/MOTIF Data Archive is supported by CEA, CNRS, the EU project MOTIF (EVK2-CT-2002-00153) and the Programme National d'Etude de la Dynamique du Climat (PNEDC). The analyses were performed using version 10/01/2006 of the database. More information is available on http://www-lsce.cea.fr/pmip/ and http://www-lsce.cea.fr/motif/.

References

Berger, A.: Long-term variations of caloric solar radiation resulting from the earth's orbital elements, Quat. Res., 9, 139–167, 1978.

Bony, S., Colman, R., Kattsov, V. M., Allan, R. P., Bretherton, C. S., Dufresne, J. L., Hall, A., Hallegatte, S., Holland, M. M., Ingram, W., Randall, D. A., Soden, B. J., Tselioudis, G., and Webb, M. J.: How well do we understand and evaluate climate change feedback processes?, J. Climate, 19, 3445–3482, 2006.

Braconnot, P., Joussaume, S., Marti, O., and de Noblet, N.: Synergistic feedbacks from ocean

and vegetation on the African monsoon response to mid-Holocene insolation, Geophys.Res. Lett., 26, 2481–2484, 1999.
Braconnot, P., Joussaume, S., de Noblet, N., and Ramstein, G.: Mid-holocene and Last Glacial Maximum African monsoon changes as simulated within the Paleoclimate Modelling Intercomparison Project, Global Planet. Change, 26, 51–66, 2000a.
Braconnot, P., Marti, O., Joussaume, S., and Leclainche, Y.: Ocean feedback in response to 6 kyr BP insolation, J. Climate, 13, 1537–1553, 2000b.
Braconnot, P., Loutre, M. F., Dong, B., Joussaume, S., and Valdes, P.: How the simulated change in monsoon at 6 ka BP is related to the simulation of the modern climate: results from the Paleoclimate Modeling Intercomparison Project, Clim. Dyn., 19, 107–121, 2002.
Braconnot, P.: Modeling the last glacial maximum and mid-holocene, Comptes Rendus Geoscience, 336, 711–719, 2004.
Braconnot, P., Harrison, S., Joussaume, J., Hewitt, C., Kitoh, A., Kutzbach, J., Liu, Z., Otto-Bleisner, B. L., Syktus, J., and Weber, S. L.: Evaluation of coupled ocean-atmosphere simulations of the mid-Holocene, Past Climate Variability through Europe and Africa, R. W. b. e. al., Ed., Kluwer Academic publisher, 2004.
Cane, M. A., Braconnot, P., Clement, A., Gildor, H., Joussaume, S., Kageyama, M., Khodri, M., Paillard, D., Tett, S., and Zorita, E.: Progress in paleoclimate modeling, J. Climate, 19, 5031–5057, 2006.
Claussen, M. and Gayler, V.: The greening of the Sahara during the mid-Holocene: results of an interactive atmosphere-biome model, Glob. Ecol. Biogeogr. Lett., 6, 369–377, 1997.
CLIMAP, 1981: Seasonal reconstructions of the Earth's surface at the last glacial maximum, Map Series Technical Report MC-36, 1981.
Crucifix, M.: Does the Last Glacial Maximum constrain climate sensitivity?, Geophys. Res. Lett., 33, L18701, doi:10.1029/2005GL027137, 2006.
Douville, H.: Detection-attribution of global warming at the regional scale: How to deal with precipitation variability?, Geophys. Res. Lett., 33, L02701, doi:10.1029/2005GL024967, 2006.
Farrera, I., Harrison, S. P., Prentice, I. C., Ramstein, G., Guiot, J., Bartlein, P. J., Bonnefille, R., Bush, M., Cramer, W., von Grafenstein, U., Holmgren, K., Hooghiemstra, H., Hope, G., Jolly, D., Lauritzen, S.-E., Ono, Y., Pinot, S., Stute, M., and Yu, G.: Tropical climates at the last glacial maximum: a new synthesis of terrestrial palaeoclimate data. I. Vegetation, lake-levels and geochemistry, Clim. Dyn., 15, 823–856, 1999.
Gadgil, S. and Sajani, S.: Monsoon precipitation in the AMIP runs, Clim. Dyn., 14, 659–689,

1998.
Ganopolski, A., Kubatzki, C., Claussen, M., Brovkin, V., and Petoukhov, V.: The influence of Vegetation-atmosphere-Ocean Interaction on Climate During the Mid-Holocene, Science, 280, 1916–1919, 1998.
Gordon, C., Cooper, C., Senior, C. A., Banks, H., Gregory, J. M., Johns, T. C., Mitchell, J. F. B., and Wood, R. A.: The simulation of SST, sea ice extents and ocean heat transports in a version of the Hadley Centre coupled model without flux adjustments, Clim. Dyn., 16, 147–168, 2000.
Haak, H., Jungclaus, J., Mikolajewicz, U., and Latif, M.: Formation and propagation of great salinity anomalies, Geophys. Res. Lett., 30, 1473, doi:10.1029/2003GL017065, 2003.
Harrison, S.: Palaeoenvironmental data set and model evaluation in PMIP. Vol. WCRP-111, WMO/TD-No. 1007, Paleoclimate Modeling Intercomparison Project (PMIP), proceedings of the Third PMIP workshop, 2000.
Harrison, S., Braconnot, P., Hewitt, C., and Stouffer, R. J.: Fourth international workshop of The Palaeoclimate Modelling Intercomparison Project (PMIP): launching PMIP Phase II., EOS, 83, 447–447, 2002.
Hewitt, C. D. and Mitchell, J. F. B.: GCM simulations of the climate of 6 kyr BP: Mean changes and interdecadal variability, J. Climate, 9, 3505–3529, 1996.
IPCC: Climate Change 2001, The Scientific Basis. Cambridge University press, 98 pp, 2001.
Jacob, R., Schafer, C., Foster, I., Tobis, M., and Andersen, J.: Computational design and performance of the fast ocean atmosphere model: version 1. In: The 2001 international conference on computational science, 175-184, 2001.
Joussaume, S. and Taylor, K. E.: Status of the Paleoclimate Modeling Intercomparison Project, in Proceedings of the first international AMIP scientific conference, WCRP-92, Monterey, USA, 425–430, 1995.
Joussaume, S., Taylor, K. E., Braconnot, P., Mitchell, J. F. B., Kutzbach, J. E., Harrison, S. P., Prentice, I. C., Broccoli, A. J., Abe-Ouchi, A., Bartlein, P. J., Bonfils, C., Dong, B., Guiot, J., Herterich, K., Hewitt, C. D., Jolly, D., Kim, J. W., Kislov, A., Kitoh, A., Loutre, M. F., Masson, V., McAvaney, B., McFarlane, N., de Noblet, N., Peltier, W. R., Peterschmitt, J. Y., Pollard, D., Rind, D., Royer, J. F., Schlesinger, M. E., Syktus, J., Thompson, S., Valdes, P., Vettoretti, G., Webb, R. S., and Wyputta, U.: Monsoon changes for 6000 years ago: Results of 18 simulations from the Paleoclimate Modeling Intercomparison Project (PMIP), Geophys. Res. Lett., 26, 859–862, 1999.

K-1-Model-Developers, 2004: K-1 coupled GCM (MIROC description)1, 34 pp, 2004.
Kageyama, M., Valdes, P. J., Ramstein, G., Hewitt, C., and Wyputta, U.: Northern hemisphere storm tracks in present day and last glacial maximum climate simulations: A comparison of the European PMIP models, J. Climate, 12, 742–760, 1999.
Kageyama, M., Laine, A., Abe-Ouchi, A., Braconnot, P., Cortijo, E., Crucifix, M., de Vernal, A., Guiot, J., Hewitt, C. D., Kitoh, A., Kucera, M., Marti, O., Ohgaito, R., Otto-Bliesner, B., Peltier, W. R., Rosell-Mele, A., Vettoretti, G., Weber, S. L., Yu, Y., and Members, M. P.: Last Glacial Maximum temperatures over the North Atlantic, Europe and western Siberia: a comparison between PMIP models, MARGO sea-surface temperatures and pollen-based reconstructions, Quat. Sci. Rev., 25, 2082–2102, 2006.
Khodri, M., Cane, M. A., Kukla, G., Gavin, J., and Braconnot, P.: The impact of precession changes on the Arctic climate during the last interglacial-glacial transition, Earth Planet. Sci. Lett., 236, 285–304, 2005.
Kucera, M., Weinelt, M., Kiefer, T., Pflaumann, U., Hayes, A., Chen, M. T., Mix, A. C., Barrows, T. T., Cortijo, E., Duprat, J., Juggins, S., and Waelbroeck, C.: Reconstruction of sea-surface temperatures from assemblages of planktonic foraminifera: multi-technique approach based on geographically constrained calibration data sets and its application to glacial Atlantic and Pacific Oceans, Quat. Sci. Rev., 24, 951–998, 2005.
Kutzbach, J. E., Guetter, P. J., Behling, P. J., and Selin, R.: Simulated climatic changes: results of the COHMAP climate-model experiments. Global climates since the Last Glacial Maximum, University of Minnesota Press, Minneapolis, 24–93, 1993.
Kutzbach, J. E. and Liu, Z.: Response of the African monsoon to orbital forcing and ocean feedbacks in the middle Holocene, Science, 278, 440–443, 1997.
Levis, S., Bonan, G. B., and Bonfils, C.: Soil feedback drives the mid-Holocene North African monsoon northward in fully coupled CCSM2 simulations with a dynamic vegetation model, Clim. Dyn., 23, 791–802, 2004.
Liu, Z., Harrison, S. P., Kutzbach, J., and Otto-Bliesner, B.: Global monsoons in the mid-Holocene and oceanic feedback, Clim. Dyn., 22, 157–182, 2004.
Manabe, S. and Broccoli, A. J.: A Comparison of Climate Model Sensitivity with Data from the Last Glacial Maximum, J. Atmos. Sci., 42, 2643–2651, 1985.
Marsland, S. J., Haak, H., Jungclaus, J. H., Latif, M., and Roske, F.: The Max-Planck-Institute global ocean/sea ice model with orthogonal curvilinear coordinates, Ocean Model., 5, 91–127, 2003.

Marti, O., Braconnot, P., Bellier, J., Benshila, R., Bony, S., Brockmann, P., Cadule, P., Caubel, A., S., D., Dufresne, J.-L., Fairhead, L., Filiberti, M.-A., Foujols, M.-A., Fichefet, T., Friedlingstein, P., Gosse, H., Grandpeix, J.-Y., Hourdin, F., Krinner, G., Lévy, C., Madec, G., Musat, I., de Noblet, N., Polcher, J., and Talandier, C.: The New IPSL climate system model: IPSL-CM4, Note du Pôle de Modélisation, 26, 1288–1619, 2005.

Masson-Delmotte, V., Kageyama, M., Braconnot, P., Charbit, S., Krinner, G., Ritz, C., Guilyardi, E., Jouzel, J., Abe-Ouchi, A., Crucifix, M., Gladstone, R., Hewitt, C., Kitoh, A., LeGrande, A., Marti, O., Merkel, U., Motoi, T., Ohgaito, R., Otto-Bliesner, B., Peltier, W., Ross, I., Valdes, P., Vettoretti, G., Weber, S., Wolk, F., and Yu, Y.: Past and future polar amplification of climate change: climate model intercomparisons and ice-core constraints, Clim. Dyn., 26, 513–529, 2006.

Meehl, G. A., Washington, W. M., Arblaster, J. M., and Hu, A. X.: Factors affecting climate sensitivity in global coupled models, J. Climate, 17, 1584–1596, 2004.

Otto-Bliesner, B. L., Brady, E. C., Clauzet, G., Tomas, R., Levis, S., and Kothavala, Z.: Last Glacial Maximum and Holocene climate in CCSM3, J. Climate, 19, 2526–2544, 2006.

Peltier, W. R.: Ice age paleotopography, Science, 265, 195–201, 1994.

Peltier, W. R.: Global Glacial isostasy and the surface ot the ice-age Earth: the ICE-5G(VM2) model and GRACE, Ann. Rev. Earth Planet. Sci., 32, 111–149, 2004.

Pinot, S., Ramstein, G., Harrison, S. P., Prentice, I. C., Guiot, J., Stute, M., and Joussaume, S.: Tropical paleoclimates at the Last Glacial Maximum: comparison of Paleoclimate Modeling Intercomparison Project (PMIP) simulations and paleodata, Clim. Dyn., 15, 857–874, 1999a.

Pinot, S., Ramstein, G., Harrison, S. P., Prentice, I. C., Guiot, J., Stute, M., Joussaume, S., and PMIP-participating-groups: Tropical paleoclimates at the Last Glacial Maximum: comparison of Paleoclimate Modeling Intercomparison Project (PMIP) simulations and paleodata, Clim. Dyn., 857–874, 1999b.

PMIP: Paleoclimate Modeling Intercomparison Project (PMIP), proceedings of the third PMIP Workshop. WCRP-111,WMO/TD-No. 1007, 271 pp, 2000.

Renssen, H., Goosse, H., Fichefet, T., Brovkin, V., Driesschaert, E., and Wolk, F.: Simulating the Holocene climate evolution at northern high latitudes using a coupled atmosphere-sea ice-ocean-vegetation model, Clim. Dyn., 24, 23–43, 2005.

Roeckner, E., Bauml, G., Bonaventura, L., Brokopf, R., Esch, M., Giorgetta, M., Hagemann, S., Kirchner, I., Kornblueh, L., Manzini, E., Rhodin, A., Schlese, U., Schulzweida, U., and Tompkins, A., 2003: The atmospheric general circulation model ECHAM5, Part I: Model

description, internal report 349, 144 pp, 2003.
Taylor, K. E., Hewitt, C., Braconnot, P., Broccoli, A. J., Doutriaux, C., Mitchell, J. F. B., and groups, P. p.: Analysis of forcing, response, and feedbacks in a paleoclimate modeling experiment, Paleoclimate Modeling Intercomparison Project (PMIP), Proceedings of the thrid PMIP Workshop, La Huardire, Canada, 271, 2000.
Taylor, K. E., Crucifix, M., Braconnot, P., Hewitt, C., Doutriaux, C., Webb, M. J., Broccoli, A. J., and Mitchell, J. F. B.: Estimating shortwave radiative forcing and response in climate models, J. Climate, press, 2006.
Texier, D., de Noblet, N., Harrison, S. P., Haxeltine, A., Jolly, D., Joussaume, S., Laarif, F., Prentice, I. C., and Tarasov, P.: Quantifying the role of biosphere-atmosphere feedbacks in climate change: coupled model simulations for 6000 years BP and comparison with palaeodata for northern Eurasia and northern Africa, Clim. Dyn., 13, 865–882, 1997.
Vries, P. and Weber, S. L.: The Atlantic freshwater budget as a diagnostic for the existence of a stable shut-down of the meridional overturning circulation, Geophys. Res. Lett., 32, L09606, doi:10.1029/2004GL021450, 2005.
Weber, S. L., Drijfhout, S. S., Abe-Ouchi, A., Crucifix, M., Eby, M., Ganopolski, A., Mukarami, D., Otto-Bleisner, B. L., and Peltier, W. R.: The modern and glacial overturning circulation in the Atlantic ocean in PMIP coupled model simulations, Clim. Past Discuss., 2, 923–949., 2006.
Wohlfahrt, J., Harrison, S. P., and Braconnot, P.: Synergistic feedbacks between ocean and vegetation on mid- and high-latitude climates during the mid-Holocene, Clim. Dyn., 22, 223–238, 2004.
Xie, P. and Arkin, P.: Analyses of global monthly precipitation using gauge observations, satellite estimates, and numerical model predictions, J. Climate, 9, 840–858, 1996.
Yu, Y. Q., Yu, R. C., Zhang, X. H., and Liu, H. L.: A flexible coupled ocean-atmosphere general circulation model, Adv. Atmos. Sci., 19, 169–190, 2002.
Yu, Y. Q., Zhang, X. H., and Guo, Y. F.: Global coupled ocean-atmosphere general circulation models in LASG/IAP, Adv. Atmos. Sci., 21, 444–455, 2004.
Yukimoto, S., Noda, A., Kitoh, A., Hosaka, M., Yoshimura, H., Uchiyama, T., Shibata, K., Arakawa, O., and Kusunoki, S.: Present-day climate and climate sensitivity in the Meteorological Research Institute coupled GCM version 2.3 (MRI-CGCM2.3), J. Meteorol. Soc. Japan, 84, 333–363, 2006.
Zhao, Y., Braconnot, P., Marti, O., Harrison, S. P., Hewitt, C., Kitoh, A., Liu, Z., Mikolajewicz, U.,

Otto-Bliesner, B., and Weber, S. L.: A multi-model analysis of the role of the ocean on the African and Indian monsoon during the mid-Holocene, Clim. Dyn., 25, 777–800, 2005.
Zhao, Y., Braconnot, P., Harrison, S., Yiou, P., and Marti, O.: Simulated changes in the relationship between tropical ocean temperatures and northwestern African summer rainfall during the mid-Holocene, Clim. Dyn., 10.1007/s00382-006-0196-7, 2006.

Table 1. Boundary conditions, trace gazes and Earth's orbital parameters as recommended by the PMIP2 project.

	Ice Sheets	Topography Coastlines	CO2 (ppmv)	CH4 (ppbv)	NO2 (ppbv)	Eccentricity	Obliquity (°)	Angular precession (°)
0 ka	Modern	Modern	280	760	270	0.0167724	23.446	102.04
6 a	Same as 0 K	Same as 0 K	280	650	270	0.018682	24.105	0.87
21 ka	ICE-5G	ICE-5G	185	350	200	0.018994	22.949	114.42

Table 2. Model characteristics and references. The last two columns indicate which time slices were performed for each model. The crosses stand for OA simulations and the circles for OAV simulations.

Model name as specified in PMIP2 database	Resolution Atm Long x lat (levels)	Resolution Ocean Long x lat (levels)	Flux Adjustment	Reference for model	6 ka	21 ka
CCSM3	T42 (26)	1°×1° (40)	None	Otto-Bliesner et al. (2005)	x	x
ECBilt-Clio	T21 (3)	3×3 (20)	Basin-mean	Vries and Weber (2005)		x
ECBilt-CLIO-VECODE	T21 (3)	3×x3 (20)		Renssen et al. (2005)	xo	
ECHAM5-MPIOM1	T31 (19)	1.875°×0.84° (40)	None	Roeckner et al. (2003); Marsland et al. (2003); Haak et al. (2003).	x	
FGOALS-g1.0	2.8x2.8 (26)	1°×1° (33)	None	Yu et al. (2002); Yu et al. (2004).	x	x
FOAM	R15 (18)	2.8°×1.4° (16)	None	Jacob et al. (2001)	xo	
HadCM3M2	3.75°×2.5° (19)	1.25°×1.25° (20)	None	Gordon et al. (2000)		xo
UBRIS-HadCM3M2	3.75°×2.5° (19)	1.25°×1.25° (20)	None	Gordon et al. (2000)	xo	
IPSL-CM4-V1-MR	2.5°×3.75° (19)	2°×0.5° (31)	None	Marti et al. (2005)	x	x
MIROC3.2	T42 (20)	1.4°×0.5° (43)	None	K-1 Model Developers (2004)	x	x
MRI-CGCM2.3fa	T42 (30)	2.5°×0.5° (23)	Yes	Yukimoto et al. (2006)	x	
MRI-CGCM2.3nfa	T42 (30)	2.5°×0.5° (23)	None	Yukimoto et al. (2006)	x	

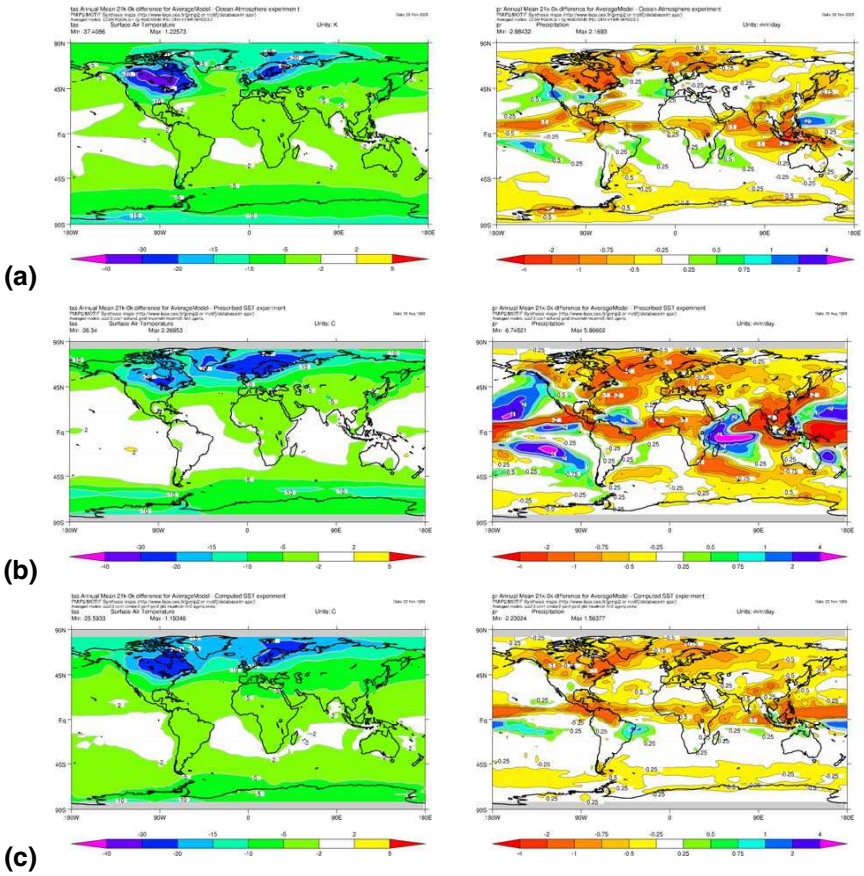

Fig. 1. Annual mean LGM change in temperature (left) and precipitation (right) for **(a)** the ensemble mean of PMIP2 simulations, **(b)** the ensemble mean of PMIP1 simulations with fixed SST and **(c)** the ensemble mean of PMIP1 simulations with computed SST.

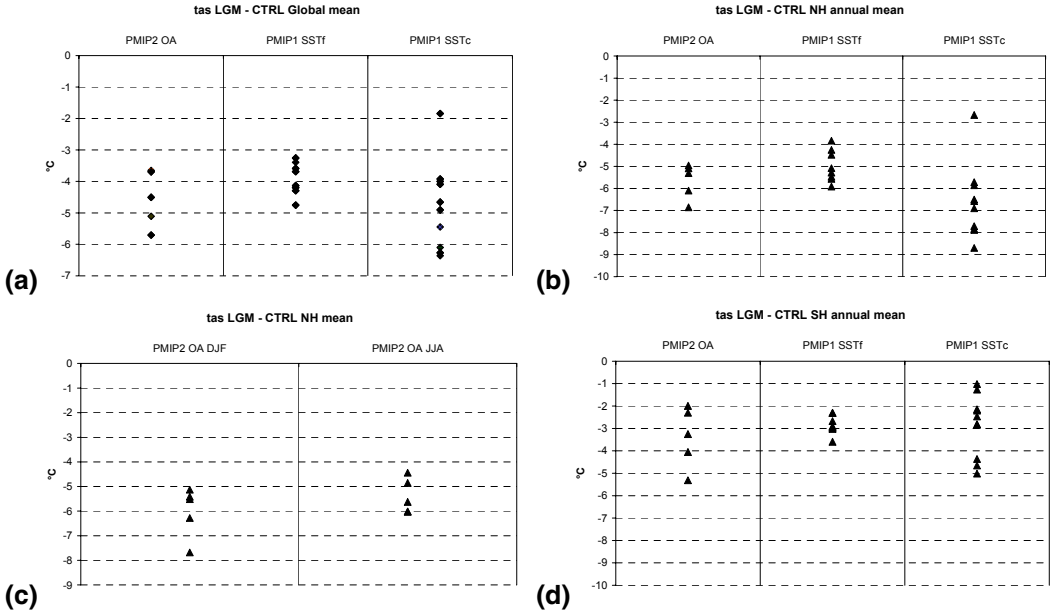

Fig. 2. Comparison of the change in surface air temperature from PMIP1 OA, PMIP1 SSTf and PMIP1 SSTc experiments for **(a)** the global annual mean, **(b)** NH annual mean, **(c)** NH June–July–August (JJA) and December–January–February (DJF) seasonal means, and **(d)** SH annual mean.

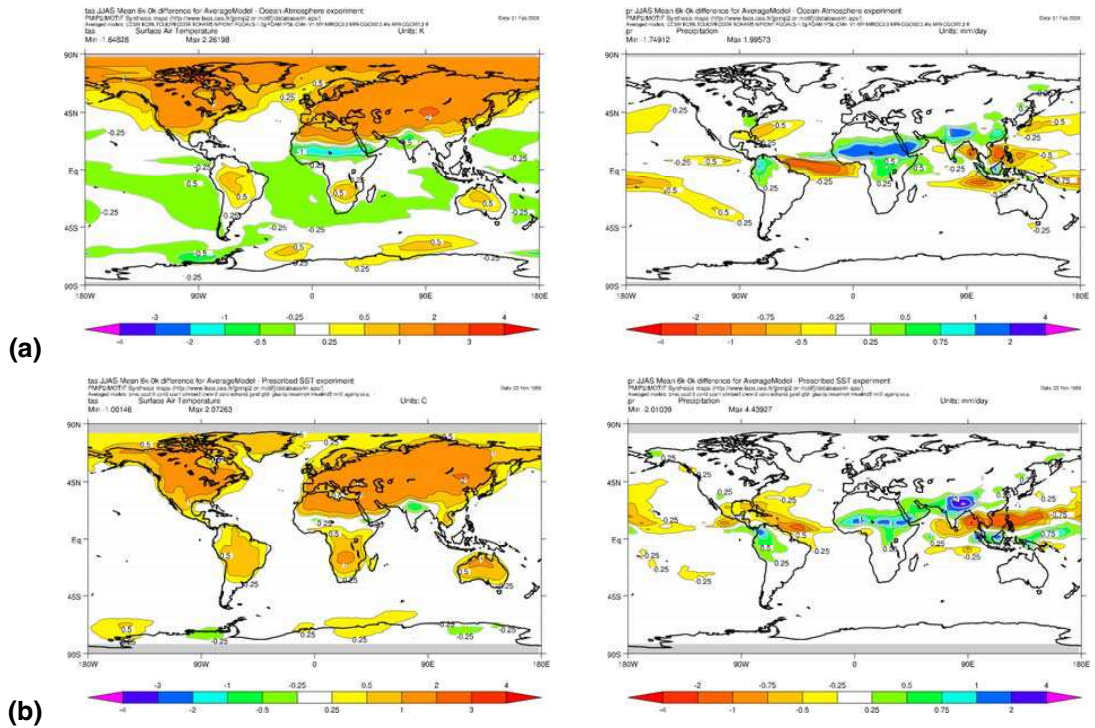

Fig. 3. JJAS mean temperature and precipitation differences between mid-Holocene and preindustrial (0k) for **(a)** the ensemble mean of PMIP2 simulations, and **(b)** the ensemble mean of PMIP1 simulations.

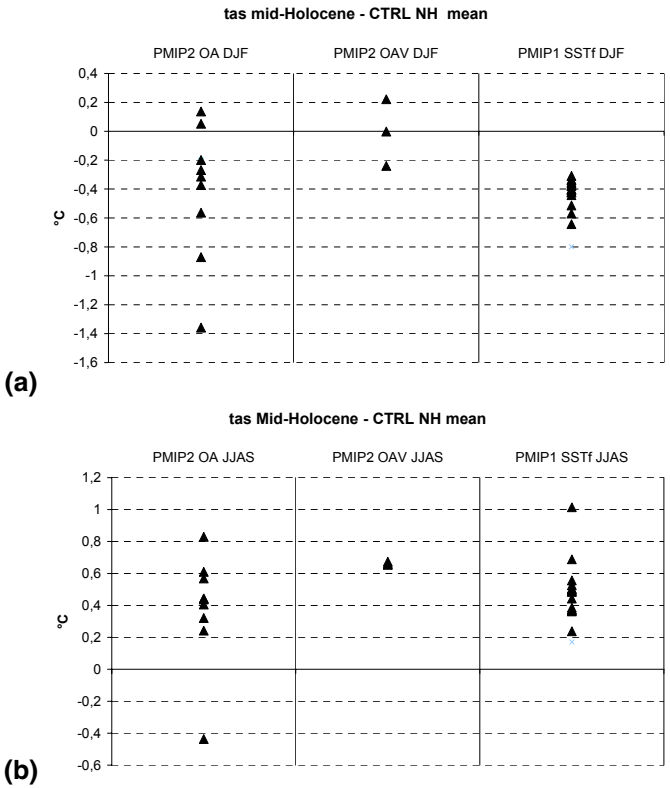

Fig. 4. As Fig. 2, but for DJF and JJAS mid-Holocene changes in air temperature averaged over NH.

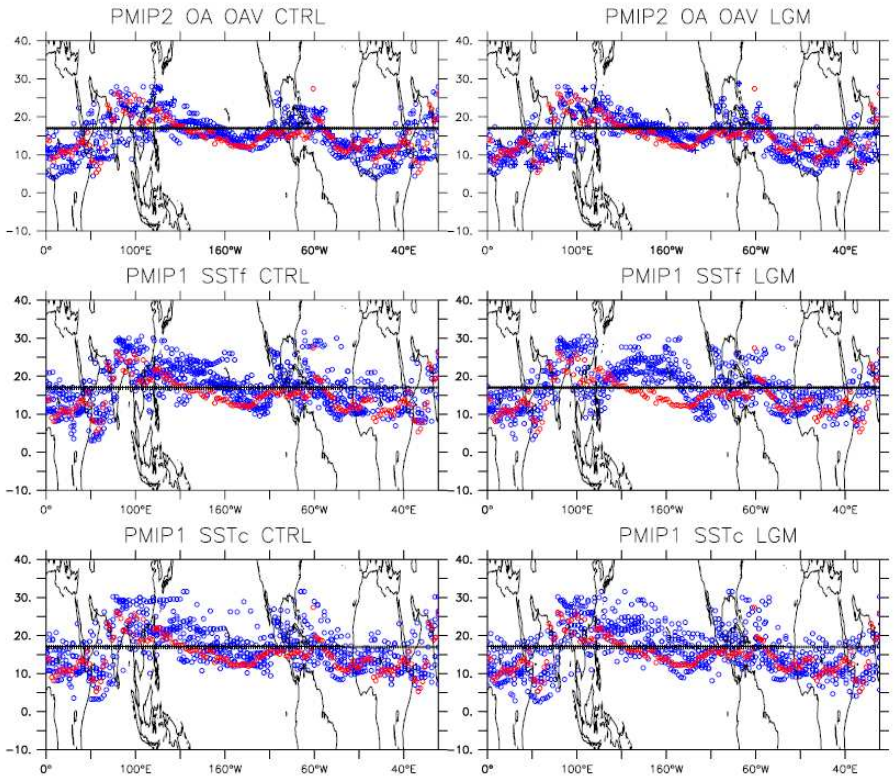

Fig. 5. Location of the ITCZ at the northern edge of its seasonal march (see text for the exact definition, and the criterion used to compute it) for pre-industrial and LGM simulations. Blue circles are the estimates from the different model results. Red circles are the reference from the CMAP climatology of precipitation. In addition the 17° N latitude is also drawn on all graphs to provide a visual reference. Plots on the left side of the figure show how the ITCZ is represented in the control simulations whereas the right side shows the location of the ITCZ simulated for the LGM. Results for PMIP2 OA, PMIP1 SSTf, and PMIP1 SSTc are respectively displayed from top to bottom panels.

CPD
2, 1293–1346, 2006

EGU

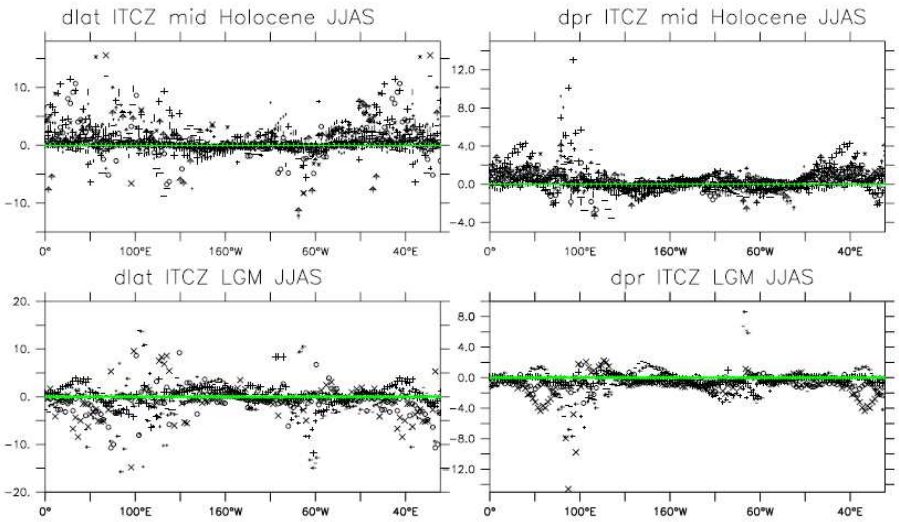

Fig. 6. Change in the northern most location of the ITCZ as simulated by PMIP2 OA simulations for **(a)** the mid-Holocene and **(c)** LGM, and change in the mean precipitation simulation in the northern part of the ITCZ for **(b)** mid Holocene, and **(d)** LGM (see text for detailed calculation). The zero line is plotted in green as a reference.

CPD
2, 1293–1346, 2006

EGU

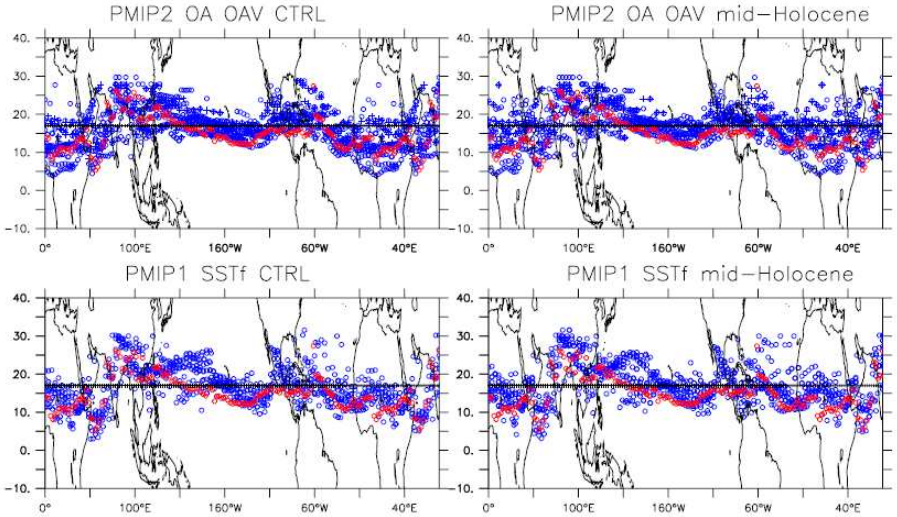

Fig. 7. Same as Fig. 5, but for mid-Holocene.

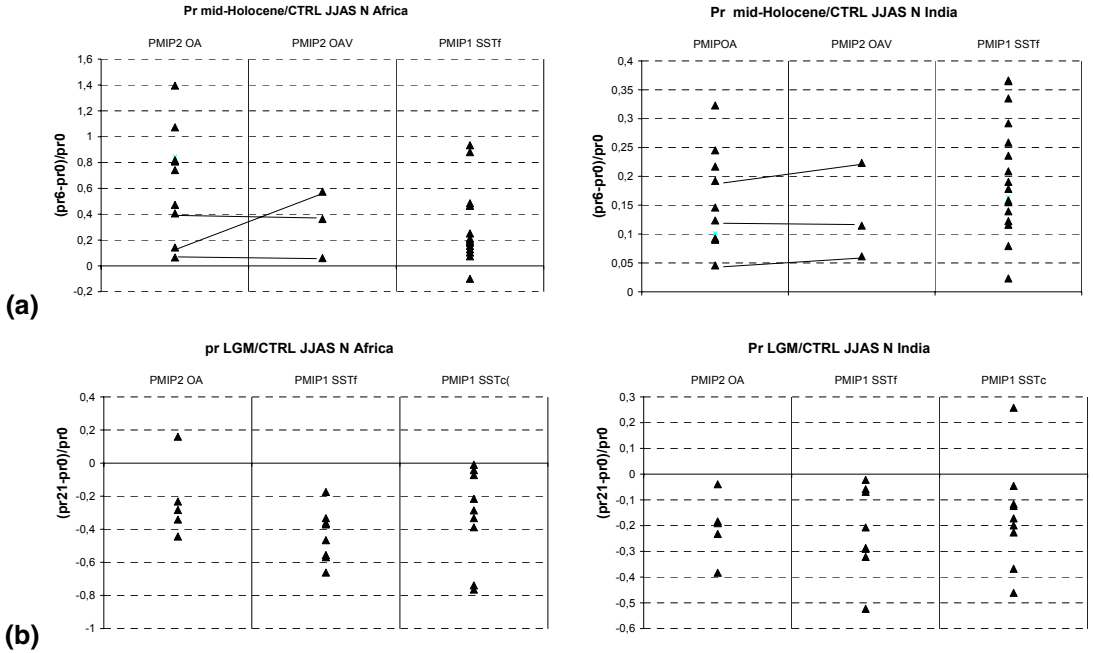

Fig. 8. Comparison of the JJAS change in precipitation simulated by PMIP2 and PMIP1 experiments respectively over Africa (20° W–30° E; 10° N–25° N) and North Indian (70° E–100° E; 20° N–40° N) for **(a)** mid-Holocene and **(b)** LGM. The lines link results of the same model when both OA and OAV simulations are available in the database.

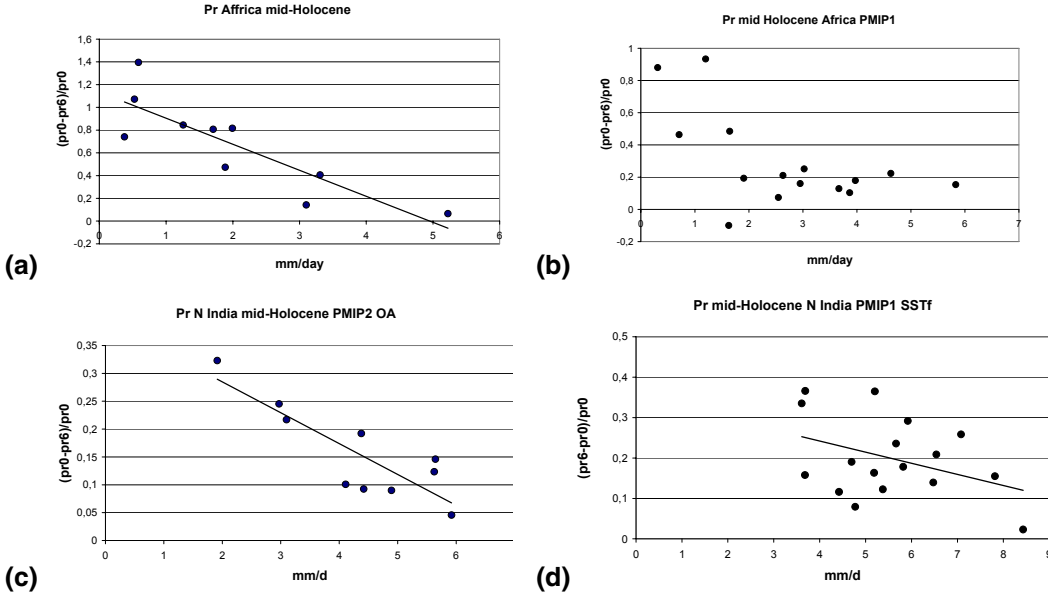

Fig. 9. Relation ship between the mid-Holocene change in precipitation (ratio to control) and control precipitation for the Sahel (top panel) and N. Indian (bottom panel) boxes and **(a)** PMIP2 OA simulations, **(b)** PMIP1 SSTf simulations, **(c)** PMIP2 OA simulations, **(d)** PMIP1 SSTf .

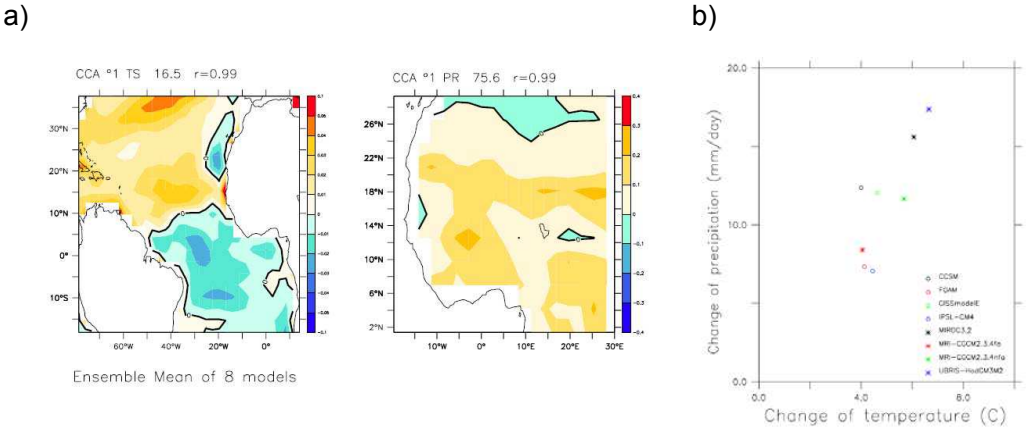

Fig. 10. Sahel precipitation amplification by the atlantic dipole for mid-Holocene, **(a)** 2nd CCA pattern of SST change in the Atlantic Ocean and of precipitation change over Africa, **(b)** relation ship between the projection of the different model results on this pattern during summer (each dot represent a model).

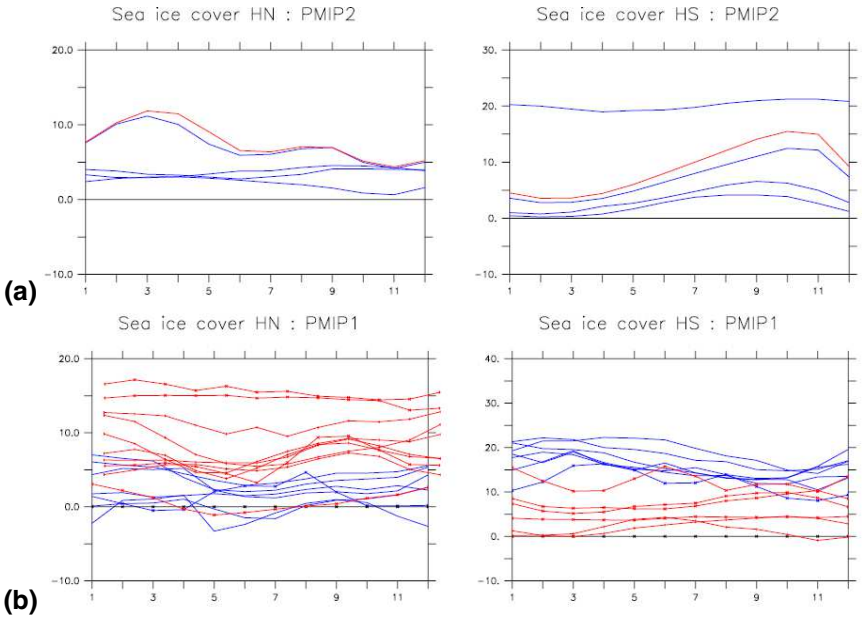

Fig. 11. Change in Sea-ice cover during LGM as a function of months for NH(left) and SH(right). **(a)** PMIP2 OA (blue) and OAV (red) experiments, **(b)** PMIP1 SSTf (blue) and SSTc (red experiments).

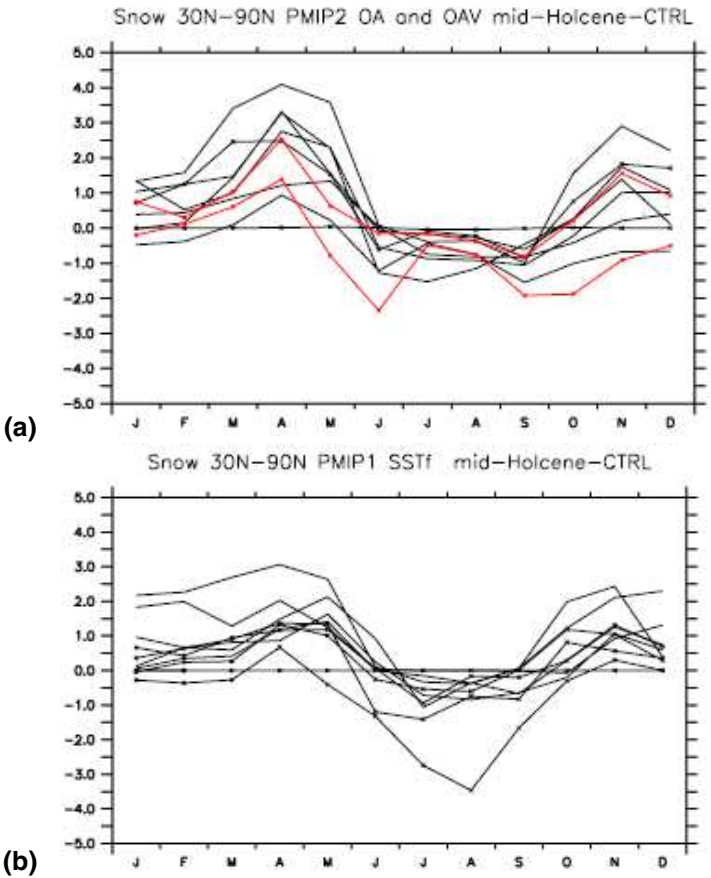

Fig. 12. Mean seasonal evolution of the change in NH snow cover simulated by **(a)** PMIP2 OA (black) and OAV (red) experiments and **(b)** PMIP1 SSTf experiments.

CPD
2, 1293–1346, 2006

EGU

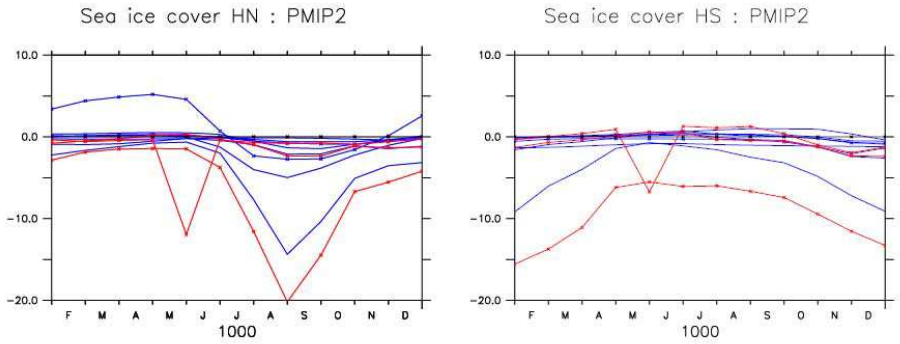

Fig. 13. Same as Fig. 11, but only for PMIP2 OA mid-Holocene simulations.

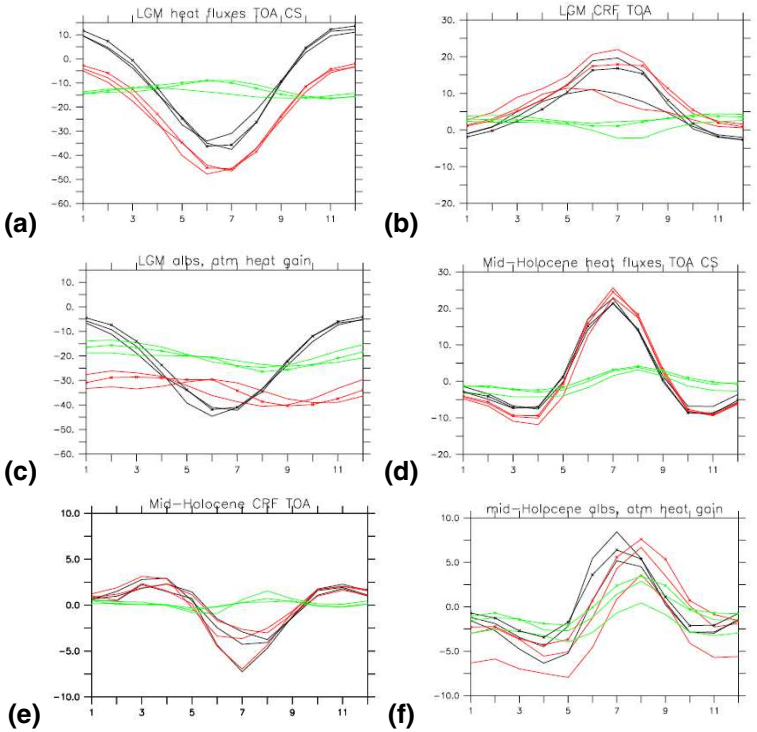

Fig. 14. Change in radiative heat budget averaged from 30° N to 90° N for a substet of PMIP2OA simulations. **(a)** changes in LGM clear sky heat budget (black, positive downward), clear sky short waver (red, positive downward) and clear sky longwave (green, outgoing radiation positive upward) **(b)** change in LGM cloud radiative forcing (black, positive down ward), with the short wave (red) and longwave (green) contributions, and **(c)** contribution of the surface albedo on the shorwave radiation (black, positive downward), change in LW emission due to change in surface temperature (red, positive upward), and change in the atmospheric heat gain (green, positive downward) for LGM. **(d)**, **(e)** and **(f)** same as (a), (b), (c), but for mid-Holocene.

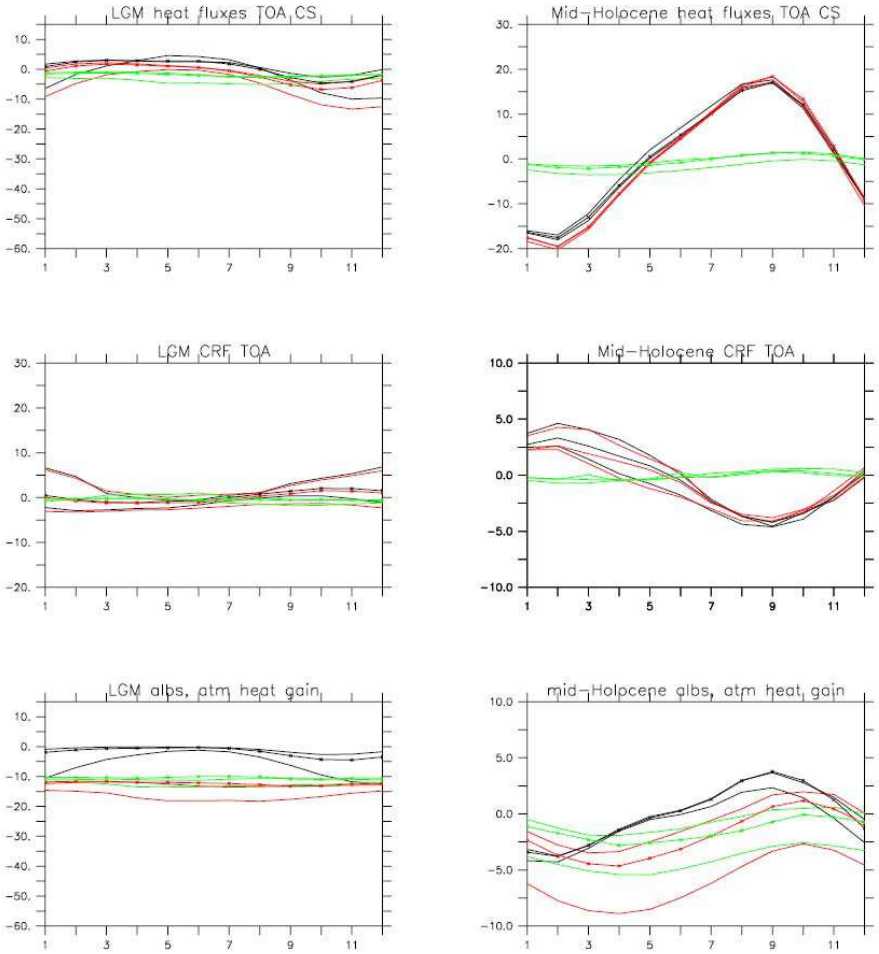

Fig. 15. Same as Fig. 14, but for SH.